Mon. Not. R. Astron. Soc. **000**, 1–?? (2016) Printed November 23, 2016 (MN LaTeX style file v2.2)

A *WISE*-based search for debris discs amongst M-dwarfs in nearby, young, moving groups

A. S. Binks[1,2⋆] and R. D. Jeffries[2]
[1] *Centro de Radioastronomía y Astrofísica, Universidad Nacional Autónoma de México, PO Box 3-72, 58090 Morelia, Michoacán, México*
[2] *Astrophysics Group, School of Chemistry and Physics, Keele University, Keele, Staffordshire ST5 5BG*

arXiv:1611.07416v1 [astro-ph.SR] 22 Nov 2016

Accepted. Received; in original form

ABSTRACT

We present a search for debris discs amongst M-dwarf members of nearby, young (5–150 Myr) moving groups (MGs) using infrared (IR) photometry, primarily from the Wide Infrared Survey Explorer (*WISE*). A catalogue of 100 MG M-dwarfs that have suitable *WISE* data is compiled and 19 of these are found to have significant IR excess emission at 22 μm. Our search is likely to be complete for discs where the ratio of flux from the disc to flux from the star $f_{\rm d}/f_* > 10^{-3}$. The spectral energy distributions are supplemented with 2MASS photometry and data at longer wavelengths and fitted with simple disc models to characterise the IR excesses. There is a bimodal distribution – twelve targets have $W1 - W4 > 3$, corresponding to $f_{\rm d}/f_* > 0.02$ and are likely to be gas-rich, primordial discs. The remaining seven targets have $W1 - W4 < 1$ ($f_{\rm d}/f_* \lesssim 10^{-3}$) and include three objects with previously known or suspected debris discs and four new debris disc candidates that are all members of the Beta Pic MG. All of the IR excesses are identified in stars that are likely members of MGs with age < 30 Myr. The detected debris disc frequency falls from 13 ± 5 per cent to < 7 per cent (at 95 per cent confidence) for objects younger or older than 30 Myr respectively. This provides evidence for the evolution of debris discs on this timescale and does not support models where the maximum of debris disc emission occurs much later in lower-mass stars.

Key words: stars: discs – stars: circumstellar matter – stars: low-mass – stars: pre-main-sequence

1 INTRODUCTION

The formation of low-mass stars is thought to inevitably involve a "primordial" disc of gas and dust. Over the course of a few Myr, this disc evolves in a poorly understood way: small dust particles form and coagulate; some gas can accrete onto the star or is expelled in winds; an inner hole may form. The progression from an optically thick primordial disc, through transitional discs with inner holes to an optically thin disc may take a few to 10 Myr (Haisch, Lada & Lada 2001; Hernández et al. 2008). At the same time, grains may grow to form planetesimals and then second generation, optically thin, debris discs may form due to collisional cascades or collisions between rocky protoplanets (Wyatt 2008).

Much of the work on the evolution of debris discs around stars has focused on coeval cohorts of known age in open clusters. The occurrence of observed debris discs appears to depend on both age and spectral-type; debris discs are more common around early-type stars and around young stars (Wyatt 2008). From 10 to 100 Myr there is a decline in debris disc frequency from ~ 40 to 10 per cent amongst solar-type stars, although a large scatter remains present throughout this range. A-type stars take ~ 500 Myr for the same level of decline (Siegler et al. 2007), in broad agreement with collisional cascade models (Kenyon & Bromley 2005; Thébault & Wu 2008).

Whilst much observational work has focused on the debris disc frequencies for solar-type stars, little is known about the evolution of M-dwarf debris discs, because most are too faint to be studied in open clusters and young, nearby field M-dwarfs are rare (Theissen & West 2014). It has been suggested that the evolution of debris discs around lower mass M-type stars could be more rapid. The timescales for dust dissipation may be shorter, partly due to enhanced stellar wind drag forces (Plavchan, Jura & Lipscy 2005; Trilling et al. 2008) and partly due to stronger photoevaporation in the extreme ultraviolet (Galván-Madrid et al. 2014).

The Wide-field Infrared Survey Explorer (*WISE*,

⋆ E-mail: a.binks@crya.unam.mx

© 2016 RAS

Wright et al. 2010) has been successful in uncovering hundreds of solar-type objects with an IR excess in the solar-neighbourhood (Patel, Metchev & Heinze 2014), however, very few young, nearby M-dwarfs have been reported with IR excesses (Avenhaus, Schmid & Meyer 2012). The frequency with which debris discs are found (hereafter termed the disc fraction) for young field M-dwarfs has been reported to be both smaller than FGK-types (Lestrade et al. 2009) and larger (Forbrich et al. 2008).

A potential alternative source of coeval lower mass stars are those belonging to nearby ($<$ 100 pc), young ($<$ 150 Myr), moving groups (MGs, Zuckerman & Song 2004). Some work has investigated the disc fractions in MGs (Simon et al. 2012; Schneider, Melis & Song 2012; Moór et al. 2016), none has been able to study large samples of M-dwarfs. Several recent surveys have identified new M-dwarf members (or candidate members) of nearby MGs (Shkolnik et al. 2009, 2012; Schlieder et al 2010, 2012; Malo et al. 2013; Gagné et al. 2014, 2015). To date, only three M-dwarf MG members are known to have debris discs, identified via scattered light images and thermal emission; AU Mic in the Beta Pic MG (BPMG, Kalas 2004; Augereau & Beust 2006; MacGregor 2014) and TWA 7 and 25 in the TW Hydrae MG (TWA, Choquet et al. 2016).

Motivated by the swathe of new M-dwarfs discovered in MGs, this work makes use of IR photometry to search for debris disc candidates among a large number of MG M-dwarfs. Near-IR photometry is available from 2*MASS* (Cutri et al. 2003), the main source of mid-IR photometry is *WISE* (Wright et al. 2010) and fluxes measured at longer wavelengths are available for some objects. §2 describes how the initial target catalog of M-dwarfs is compiled. The collated *WISE* photometry is presented in §3 with a description of the photometric criteria required for the detection of an IR excess. In §4 SED models and simple blackbody fits are made to stars qualifying from the photometric selection in §3. A discussion of the sensitivity limits for *WISE* detection of debris discs is presented in §5. In §6 we make assessments of the nature of the IR excess for each target with significant IR excess and we discuss previously confirmed M-dwarf debris disc systems in MGs. In §7 we present the results from our IR search and discuss its limitations. A summary is provided in §8.

2 TARGET SELECTION

2.1 Moving group membership confirmation

Recent large-scale kinematic surveys have revealed hundreds of new candidate MG M-dwarfs, many of which require follow-up data to confirm their membership status. Some searches (e.g., Schlieder, Lépine & Simon 2012) use proper motions to identify possible comoving stars with a MG and then perform follow-up spectroscopy to measure ages and kinematics, identifying likely coeval and comoving objects as MG candidates. Another approach is to identify candidate young stars based on general youth-indicators such as UV and/or X-ray activity (Shkolnik et al. 2012) or rapid rotation (Binks, Jeffries & Maxted 2015) and then acquire spectroscopy to confirm youth and test their kinematics for membership with known MGs. An alternative method based on Bayesian inference techniques compares the proper motions, positions and colours of a sample of Hα-emitting stars with the distributions observed in known MGs (e.g., Malo et al. 2013). Table 1 lists the 9 MGs considered in this work and the source paper(s) from which candidates for this paper are selected. Ages are adopted from Bell, Mamajek & Naylor (2015), unless otherwise stated in Table 1.

MG name	Age (Myr)	$N_{\rm initial}$	Source reference
ϵ Cha	3–5[a]	16	1
TWA	10 ± 3	33	2, 3, 4
η Cha	11 ± 3	12	5
BPMG	24 ± 3	45	3, 6, 7, 8, 9, 10, 11, 12, 13
Argus	30–50[b]	12	3, 14
Columba	42^{+6}_{-4}	17	3
Carina	45^{+11}_{-7}	4	3
Tuc-Hor	45 ± 4	116	3, 15
ABDMG	149^{+51}_{-19}	31	3, 9, 10, 13, 16

Table 1. MGs considered in this work. Ages are from Bell, Mamajek & Naylor (2015) except for a: Murphy, Lawson & Bessell (2013) and b: Malo et al. (2013). $N_{\rm initial}$ gives the number of M-dwarfs in each MG which satisfied all criteria for inclusion provided in §2.1. Sources references: 1) Murphy, Lawson & Bessell (2013), 2) Nakajima & Morino (2012), 3) Malo et al. (2013), 4) Ducourant et al. (2014), 5) Luhman (2004), 6) Barrado y Navascués et al. (1999), 7) Zuckerman et al. (2001), 8) Schlieder, Lépine & Simon (2010), 9) Schlieder, Lépine & Simon (2012), 10) Shkolnik et al. (2012), 11) Malo et al. (2014b), 12) Binks & Jeffries (2014), 13) Binks & Jeffries (2016) 14) De Silva et al. (2013), 15) Kraus et al. (2014), 16) Zuckerman, Song & Bessell (2004).

All 286 of the selected targets have proper-motions that are reported to be consistent with MG membership in the source paper and we also require that an object has an M-type spectral classification. If a candidate has a measured radial velocity (RV), MG membership is tested by comparing the RV of a candidate and the RV it would be expected to have were it a member – given by $V_{\rm T}\cos\lambda$, where $V_{\rm T}$ is the total speed of the MG and λ is the angle between the target's position and the MG convergent point. Convergent points are extracted from table 7 in Binks, Jeffries & Maxted (2015). If $|{\rm RV} - V_{\rm T}\cos\lambda| > 5\,{\rm km\,s^{-1}}$ then the target is rejected as a MG candidate. The sample is inevitably inhomogeneous, but where available, all kinematic information is consistent with MG membership.

2.2 Selection criteria using *WISE*

WISE (Wright et al. 2010) is a satellite-based IR telescope which mapped $>$ 99 per cent of the sky at 3.4, 4.6, 12 and 22 μm ($W1, W2, W3, W4$) with angular resolutions of 6.1", 6.4", 6.5" and 12.0", respectively. It is capable of providing 5σ point-source sensitivities of 0.068, 0.098, 0.86 and 5.4 mJy, which is two orders-of-magnitude deeper than previous satellite-based mid-IR surveys such as *IRAS*.

To obtain a reliable sample of mid-IR photometry for disc identification, targets were only retained if they had signal-to-noise ratios (SNRs) greater than 5.0 in the *WISE* $W4$ band (hereafter, SNR refers exclusively to the $W4$ band). Whilst an IR excess can be indicative of a debris disc, there are a number of false positive signals that we sought

to eliminate following guidelines in Patel, Metchev & Heinze (2014). Firstly, since interstellar cirrus near the Galactic plane can strongly contaminate *WISE* images, any objects with $l \leqslant 5^{\circ}$ are excluded. Searching the SIMBAD database, we ensured that no objects in our sample matched any of the following object descriptions that could be false-positive sources of IR-excess: post-AGB stars, white dwarfs, carbon stars, novae, Cepheids, cataclysmic variables, high-mass X-ray binaries, planetary nebulae or Wolf-Rayet stars. We then removed objects that had projected companions with $\Delta K_s \leqslant 5$ mag within 16" in 2*MASS*; this is a strict criterion but one deemed necessary to exclude contamination by extremely red, unresolved sources in *WISE*. In order to include only objects with non-variable photometry, which could affect our determination of *WISE* colours, we removed 8 stars whose *AllWISE* photometry deviates from the mean of the single exposure measurements (from the *AllWISE* L1b catalog[1]) by more than 2σ, where σ represents one standard deviation in $W1$ or $W2$ from the single frame exposures. In one case (WISE J112117.15−344645.4), the difference in $W1$ and $W2$ magnitudes between *AllWISE* and the mean of the L1b images is ~ 0.8 mag ($\sim 6\sigma$). In addition the sample was limited to objects with $W1 > 4.5$ mag and $W2 > 2.8$ to avoid saturation. To avoid contamination by known 2*MASS* extended sources, we include only stars with *WISE* `ext_flg` = 0 or 1. We include only *WISE* sources indicative of unconfused photometry: i.e., only stars with `cc_flg[Wi]` = 0 (or flagged with a lower-case initial). Finally, in an attempt to exclude variable sources, we include only objects with consistent variability detections in $W1$ and $W2$, excluding stars whose `var_flag[W1]` > 8 and `var_flag[W2]` < 5 or `var_flag[W1]` < 5 and `var_flag[W2]` > 8 (see Patel, Metchev & Heinze 2014 for an extensive description of this criterion).

Of the 286 candidate M-dwarf members in the nine MGs, 133 have SNR > 5.0; 10 in ϵ Cha, 8 in η Cha, 22 in TWA, 33 in BPMG, 2 in Carina, 5 in Columba, 26 in Tuc-Hor, 9 in Argus and 18 in ABDMG. Of these objects, 100 satisfy all the additional criteria described in this section, and these are listed in Table 2.

2.3 Flux conversion

JHK photometry is from the 2*MASS* catalog (Cutri et al. 2003) and magnitudes were converted to fluxes (all in units of erg/s/cm^2/Å) using the 2*MASS* isophotal bandpasses and zero-point magnitude fluxes from table 2 in Cohen, Wheaton & Megeath (2003). For the *WISE* data, zero-magnitude fluxes are taken from Jarrett et al. (2011) and colour corrections are available in Wright et al. (2010). Following the work in Theissen & West (2014) and the advisory notes in Wright et al. (2010), $W4$ fluxes are reduced by 10 per cent. For objects with a significant $W4$ excess (see §3), additional photometry/flux values were searched for in the *IRAS*, *AKARI*, *Spitzer IRAC* and *Spitzer MIPS*, *Herschel SPIRE* and *Herschel PACS* and *SCUBA*2 catalogs and any additional fluxes are listed in Table 4. The fluxes for *IRAS* sources were extracted directly from the *IRAS* point source catalog (Helou & Walker 1988). For the *AKARI IRC* bands (9 and 18 μm), zero magnitude fluxes are from table 8 in Tanabé et al. (2008) and the *AKARI FIS* (90 μm), the *Spitzer IRAC* and *Spitzer MIPS* zero magnitude fluxes were extracted from the calibration tables available at `http://irsa.ipac.caltech.edu/`. For *Herschel PACS* and *SPIRE* and *SCUBA*2 data, fluxes are taken directly from the source papers listed in the footnotes of Table 4.. All fluxes redward of the K band have a 10 per cent calibration error added in quadrature to the photometric uncertainties.

3 IDENTIFYING IR-EXCESS

In this section we discuss only how an IR excess was identified, delaying discussion of the possible cause of an IR excess until §6. We define two quantities E_{W3} and E_{W4} that define the significance of any IR excess over that expected from the photosphere in the respective *WISE* wavebands. These are calculated by subtracting the photospheric flux expected for a star of that spectral-type from the observed flux and then dividing by the uncertainty in the observed flux. The photospheric flux was estimated by interpolating the W_{1-4} photometry in table 5 from Pecaut & Mamajek (2013) for candidates younger than 30 Myr, or from their table 4 for candidates older than 30 Myr. The flux error is derived as the quadrature sum of the W_x photometric uncertainty and the scatter in $W1 - Wx$ for a disc-less star at a given spectral-type (from a sample of field M-dwarfs from the third catalogue of nearby stars; Gliese & Jahreiss 1991). Following Kennedy & Wyatt (2012), objects with $E_{W4} > 3.0$ are classed as having significant excess and these are discussed in more detail in §6.

Schneider, Melis & Song (2012) apply a criteria of $W1-W4 > 1.0$ mag to identify circumstellar discs around M-dwarf TWA members. From a sample of M-dwarfs from the third catalogue of nearby stars (Gliese & Jahreiss 1991) a typical colour for an M-dwarf field star without an excess is $W1 - W4 \sim 0$ with a range of ~ 0.3 mag (see below); therefore $W1-W4 = 1.0$ represents a $\sim 3\sigma$ separation from the field star sample. The range in $W1 - W3$ for M-dwarf field stars is ~ 0.15 mag, centered about 0.

Figure 1 shows a variety of colour-colour diagrams for the MG sample. A sample of primordial and transitional discs in the Taurus star-forming region (Esplin, Luhman & Mamajek 2014) is also shown and can be used to judge the efficacy of the diagrams and whether they are capable of distinguishing transitional from primordial discs. Figure 1 shows that $W1 - W4$ is likely to be the best colour indicator to pick out objects with discs. This work will utilise the same photometric colour cut as Schneider, Melis & Song (2012), however should an object with $W1 - W4 < 1.0$ have an $E_{W4} > 3.0$, then they are also assumed to be debris disc candidates, unless there is evidence to suggest otherwise.

Twelve objects survive the $W1 - W4 > 1.0$ cut: 5 in ϵ Cha, 5 in η Cha and 2 in TWA (see Table 4) and their nature is discussed in §6.1. A further seven objects have $W1 - W4 < 1.0$ and $E_{W4} > 3.0$ and these are discussed in §6.2. As a further check on the reliability of these sources, postage stamp *AllWISE* images in the $W4$ band were ex-

[1] available at `http://irsa.ipac.caltech.edu/holdings/catalogs.html`

Table 2. RV and photometric data for the 100 objects that satisfy both the RV criteria described in §2 and additional criteria in §2.2 and have SNR > 5.0 in the $W4$ band. The M-dwarf spectral-type (SpT) sub-classes are from the source paper, radial velocities (RVs) are extracted from the literature source (see §2) and $\mathrm{RV_p} = \mathrm{RV} - V_\mathrm{T}\cos\lambda$, unless there is no published RV, in which case $\mathrm{RV_p} = V_\mathrm{T}\cos\lambda$. Errors for $J, H, K, W1, W2$ and $W3$ magnitudes are usually $0.01 - 0.03$ and are always < 0.10. E_{W3} and E_{W4} are the significance of any photospheric excess in the $W3$ and $W4$ bands, respectively. Objects in bold have $W1 - W4 > 1.0$.

Name (2MASS-)	SpT M-	RV ($\mathrm{km\,s^{-1}}$)	$\mathrm{RV_p}$ ($\mathrm{km\,s^{-1}}$)	Name (WISE-)	$W1$ (mag)	$W2$ (mag)	$W3$ (mag)	$W4$ (mag, SNR)	E_{W3}	E_{W4}
				ϵ Cha ($3-5$ Myr)						
J11183572−7935548	**4.5**	$+19.3 \pm 1.6$	$+4.2$	**J111835.64−793554.8**	**9.44**	**9.14**	**7.66**	$\mathbf{4.47 \pm 0.02, 45.1}$	**27.2**	**46.5**
J11432669−7804454	**4.7**	$+15.6 \pm 1.0$	$+0.9$	**J114326.57−780445.5**	**10.22**	**9.83**	**8.68**	$\mathbf{7.05 \pm 0.07, 15.3}$	**24.8**	**14.4**
J11474812−7841524	3.0	$+16.1 \pm 0.9$	$+1.5$	J114748.00−784152.6	8.47	8.33	8.20	$8.09 \pm 0.18, 6.2$	2.3	0
J11493184−7851011	**0.0**	$+13.4 \pm 1.3$	-1.2	**J114931.74−785101.0**	**8.17**	**7.61**	**4.54**	$\mathbf{1.83 \pm 0.01, 88.8}$	**34.7**	**98.3**
J11550485−7919108	**3.0**	$+14.0 \pm 1.3$	-0.5	**J115504.71−791911.0**	**9.89**	**9.66**	**9.31**	$\mathbf{7.16 \pm 0.10, 10.9}$	**10.7**	**18.1**
J12005517−7820296	**5.8**	$+10.7 \pm 1.3$	-3.6	**J120055.08−782029.5**	**10.64**	**10.17**	**8.51**	$\mathbf{6.58 \pm 0.05, 20.8}$	**29.1**	**22.2**
J12020369−7853012	0.0	$+11.0 \pm 6.0$	-3.3	J120203.59−785301.3	8.11	8.04	7.91	$7.79 \pm 0.15, 7.5$	1.9	0
J12202177−7407393	0.0	$+12.3 \pm 0.4$	13.7	J122021.70−740739.5	8.28	8.15	8.03	$7.97 \pm 0.18, 6.0$	3.5	0
				TWA (10 ± 3 Myr)						
J02224418−6022476	4.0	$+13.1 \pm 0.9$	$+1.3$	J022244.32−602247.7	7.95	7.80	7.68	$7.50 \pm 0.12, 9.2$	1.0	0.2
J10423011−3340162	2.0	$+11.4 \pm 0.0$	-2.9	J104230.01−334016.4	6.79	6.66	6.60	$6.00 \pm 0.05, 21.4$	0.7	16.1
J11132622−4523427	0.0	$+15.8 \pm 2.0$	-2.7	J111326.18−452342.8	8.37	8.27	8.18	$8.13 \pm 0.19, 5.7$	1.6	0.3
J11315526−3436272	2.0	$+12.7 \pm 3.8$	-1.3	J113155.20−343627.3	6.66	6.44	6.41	$6.24 \pm 0.06, 19.1$	2.6	0.2
J11321831−3019518	**5.0**	$+15.8 \pm 2.0$	$+2.7$	**J113218.24−301952.0**	**8.82**	**8.44**	**7.07**	$\mathbf{5.14 \pm 0.03, 39.3}$	**26.7**	**36.8**
J12072738−3247002	3.0	$+8.5 \pm 1.2$	-0.3	J120727.32−324700.4	7.61	7.49	7.40	$7.24 \pm 0.09, 12.1$	0.3	0.7
J12073346−3932539	**8.0**	$+11.2 \pm 2.0$	$+1.6$	**J120733.42−393254.2**	**11.57**	**11.02**	**9.47**	$\mathbf{8.12 \pm 0.17, 6.2}$	**28.1**	**7.6**
J12313807−4558593	3.0	$+8.1 \pm 4.0$	-0.5	J123138.03−455859.6	8.34	8.20	8.07	$7.79 \pm 0.13, 8.7$	2.3	1.9
J12345629−4538075	1.5	$+9.0 \pm 0.4$	$+0.4$	J123456.26−453807.7	7.94	7.86	7.75	$7.54 \pm 0.12, 9.1$	1.0	0.8
J22440873−5413183	4.0	$+1.6 \pm 1.6$	$+1.0$	J224408.79−541319.0	8.30	8.14	8.01	$7.77 \pm 0.18, 6.2$	1.6	0
J23261069−7323498	0.0	$+8.0 \pm 1.9$	$+0.7$	J232610.84−732350.5	7.86	7.81	7.71	$7.61 \pm 0.13, 8.5$	0.3	0
				η Cha (11 ± 3 Myr)						
J08413030−7853064	**4.8**	**0**	**17.3**	**J084130.24−785306.3**	**10.72**	**10.35**	**8.99**	$\mathbf{7.37 \pm 0.10, 11.4}$	**26.6**	**14.7**
J08422710−7857479	**4.0**	**0**	**17.3**	**J084227.02−785747.7**	**9.72**	**9.47**	**7.86**	$\mathbf{5.19 \pm 0.03, 37.7}$	**28.0**	**39.3**
J08422372−7904030	1.8	0	17.3	J084223.64−790402.7	8.52	8.44	8.32	$7.77 \pm 0.12, 8.9$	5.2	12.3
J08431857−7905181	**3.3**	**0**	**17.3**	**J084318.52−790518.0**	**8.60**	**7.88**	**5.52**	$\mathbf{3.41 \pm 0.02, 66.8}$	**33.6**	**67.0**
J08440914−7833457	**5.8**	**0**	**17.4**	**J084409.09−783345.6**	**11.21**	**10.70**	**9.04**	$\mathbf{7.21 \pm 0.07, 15.0}$	**29.4**	**15.1**
J08441637−7859080	**4.5**	**0**	**17.3**	**J084416.33−785907.8**	**9.11**	**8.75**	**7.23**	$\mathbf{5.47 \pm 0.03, 36.6}$	**28.0**	**38.2**
J08443188−7846311	1.0	$+15.0 \pm 1.1$	-2.3	J084431.82−784630.9	8.60	8.59	8.45	$8.25 \pm 0.18, 6.2$	0	0
J08475676−7854532	3.3	0	17.3	J084756.68−785452.9	8.31	8.16	8.01	$8.03 \pm 0.15, 7.4$	2.8	0
				BPMG (24 ± 3 Myr)						
J00172353−6645124	2.5	$+10.7 \pm 0.2$	-0.2	J001723.69−664512.4	7.59	7.50	7.40	$7.34 \pm 0.13, 8.2$	0.2	0
J01112542+1526214	5.0	$+3.1 \pm 1.6$	-0.3	J011125.54+152620.7	8.02	7.79	7.63	$7.47 \pm 0.12, 8.9$	2.9	0
J01132817−3821024	3.0	$+14.3 \pm 0.5$	$+2.4$	J011328.27−382102.9	7.46	7.46	7.36	$7.19 \pm 0.11, 10.2$	0	0
J01351393−0712517	4.0	$+6.5 \pm 1.8$	-2.7	J013513.98−071251.9	7.97	7.80	7.68	$7.46 \pm 0.14, 8.0$	1.6	1.1
J01535076−1459503	4.0	$+10.5 \pm 0.4$	-1.5	J015350.81−145950.6	6.79	6.72	6.67	$6.59 \pm 0.05, 20.1$	0	0
J04593483+0147007	0.0	$+19.8 \pm 0.0$	$+1.5$	J045934.85+014659.7	6.21	6.06	6.06	$6.01 \pm 0.05, 22.0$	0.2	0
J05004714−5715255	0.5	$+19.4 \pm 0.3$	$+0.4$	J050047.16−571524.7	6.16	6.04	6.06	$5.92 \pm 0.03, 31.7$	0	0
J05335981−0221325	3.0	$+22.0 \pm 1.3$	-3.2	J053359.82−022132.9	7.54	7.43	7.34	$7.41 \pm 0.19, 5.6$	0	0
J06131330−2742054	4.0	$+22.5 \pm 0.2$	$+0.9$	J061313.30−274205.6	7.01	6.82	6.77	$6.64 \pm 0.06, 17.5$	0	0.1
J08173943−8243298	4.5	$+15.6 \pm 1.5$	$+2.8$	J081738.97−824328.8	6.48	6.27	6.22	$6.05 \pm 0.04, 29.2$	0.7	3.3
J10172689−5354265	6.0	$+13.6 \pm 0.3$	$+0.3$	J101726.70−535426.5	7.44	7.27	7.15	$7.18 \pm 0.09, 11.6$	0	4.1
J13545390−7121476	2.5	$+5.7 \pm 0.2$	-1.6	J135453.61−712148.9	7.61	7.49	7.38	$7.39 \pm 0.12, 9.3$	1.9	0
J16572029−5343316	3.0	$+1.4 \pm 0.2$	$+3.4$	J165720.25−534332.4	7.68	7.57	7.48	$7.33 \pm 0.13, 8.2$	0	0
J17173128−6657055	3.0	$+2.7 \pm 1.8$	-0.1	J171731.26−665706.8	7.53	7.36	7.20	$6.94 \pm 0.09, 11.7$	4.1	3.1
J17292067−5014529	3.0	-0.4 ± 0.0	-3.3	J172920.64−501453.4	7.81	7.68	7.56	$7.58 \pm 0.18, 6.2$	4.3	4.1
J18420694−5554254	3.0	$+0.3 \pm 0.5$	$+1.5$	J184206.97−555426.2	8.49	8.33	8.25	$7.81 \pm 0.16, 6.8$	1.3	0
J18465255−6210366	1.0	$+2.4 \pm 0.1$	$+1.2$	J184652.56−621037.3	7.75	7.71	7.62	$7.52 \pm 0.15, 7.4$	0	0
J19560294−3207186	4.0	-3.7 ± 2.2	$+4.1$	J195602.95−320719.3	7.92	7.76	7.67	$7.47 \pm 0.17, 6.4$	0.3	0
J19560438−3207376	0.0	-7.2 ± 0.5	$+0.6$	J195604.39−320738.3	7.71	7.74	7.66	$7.31 \pm 0.12, 9.1$	0	1.1
J20100002−2801410	2.5	-5.8 ± 0.6	$+2.7$	J201000.06−280141.6	7.61	7.45	7.36	$7.18 \pm 0.14, 7.6$	2.6	0.4
J20333759−2556521	3.0	-7.6 ± 0.4	$+0.5$	J203337.63−255652.8	8.68	8.44	8.32	$7.76 \pm 0.17, 6.5$	4.1	0
J20434114−2433534	3.7	-5.8 ± 0.6	$+2.1$	J204341.18−243353.8	7.58	7.44	7.39	$7.07 \pm 0.11, 9.8$	0	0.8

Table 2 – *continued*

Name (2MASS-)	SpT M-	RV ($\mathrm{km\,s^{-1}}$)	$\mathrm{RV_p}$ ($\mathrm{km\,s^{-1}}$)	Name (WISE-)	$W1$ (mag)	$W2$ (mag)	$W3$ (mag)	$W4$ (mag, SNR)	E_{W3}	E_{W4}
J20450949−3120266	1.0	-4.1 ± 0.0	+1.9	J204509.76−312030.9	4.50	4.01	4.31	$4.14 \pm 0.03, 42.3$	1.3	3.4
J21100535−1919573	2.0	-5.7 ± 0.4	+2.2	J211005.41−191958.4	7.02	7.00	6.93	$6.78 \pm 0.10, 10.9$	0	0
J22004158+2715135	0.0	-13.3 ± 2.4	−0.5	J220041.64+271513.4	7.60	7.60	7.54	$7.28 \pm 0.11, 9.8$	0	0.5
J22450004−3315258	5.0	$+2.0 \pm 0.0$	+0.5	J224500.20−331527.2	7.63	7.44	7.30	$7.18 \pm 0.10, 10.6$	1.0	0.4
J23172807+1936469	3.5	-3.7 ± 0.0	+2.7	J231728.40+193645.7	6.96	6.85	6.77	$6.58 \pm 0.06, 17.6$	0	0
J23323085−1215513	0.0	$+1.2 \pm 0.6$	+0.4	J233230.95−121552.0	6.51	6.37	6.39	$6.21 \pm 0.06, 19.2$	0	0
				Argus ($30 - 50$ Myr)						
J00503319+2449009	3.5	$+6.0 \pm 1.1$	+2.0	J005033.39+244900.3	6.87	6.70	6.64	$6.47 \pm 0.07, 16.6$	0.3	0.5
J03033668−2535329	0.0	$+20.1 \pm 0.8$	+4.0	J030336.86−253531.6	7.00	7.00	6.93	$6.81 \pm 0.06, 17.8$	0	0
J05090356−4209199	3.5	$+16.8 \pm 1.7$	−1.7	J050903.58−420919.2	8.60	8.43	8.32	$8.19 \pm 0.16, 6.8$	1.9	0
J06134539−2352077	3.5	$+22.9 \pm 0.2$	−0.5	J061345.36−235206.3	7.36	7.16	7.04	$6.51 \pm 0.06, 18.8$	3.2	0.8
J15553178+3512028	4.0	-15.5 ± 0.7	+2.1	J155531.60+351204.3	7.83	7.69	7.54	$7.37 \pm 0.09, 12.6$	1.6	0
J18450097−1409053	5.0	-23.0 ± 0.3	+1.1	J184500.95−140905.9	7.05	6.94	6.87	$6.58 \pm 0.07, 15.2$	0	0.6
J19312434−2134226	2.5	-25.6 ± 1.5	+3.8	J193124.38−213423.8	7.71	7.59	7.52	$7.37 \pm 0.15, 7.1$	0.2	0
J20163382−0711456	0.0	-23.0 ± 0.2	+1.8	J201633.88−071145.5	7.59	7.59	7.53	$7.49 \pm 0.16, 6.8$	0	0
				Columba (42^{+6}_{-4} Myr)						
J03413724+5513068	0.5	-3.2 ± 0.6	−1.4	J034137.39+551305.7	7.43	7.44	7.35	$7.27 \pm 0.11, 10.0$	0	0
J04515303−4647309	0.0	$+24.0 \pm 0.8$	+2.0	J045153.05−464730.8	8.79	8.72	8.60	$8.25 \pm 0.19, 5.8$	1.6	0
J05100488−2340148	2.0	$+24.4 \pm 0.2$	+1.4	J051004.90−234015.1	8.38	8.23	8.14	$8.10 \pm 0.19, 5.7$	2.3	0
J07065772−5353463	0.0	$+22.4 \pm 0.6$	−0.5	J070657.72−535345.9	7.56	7.57	7.48	$7.33 \pm 0.08, 13.7$	0	0
				Carina (45^{+11}_{-7} Myr)						
J06112997−7213388	4.0	$+6.0 \pm 1.1$	+2.0	J061130.01−721338.2	8.55	8.36	8.23	$8.17 \pm 0.11, 10.3$	2.6	0
J09032434−6348330	0.5	$+20.7 \pm 0.4$	−0.1	J090324.30−634832.9	8.57	8.53	8.42	$8.19 \pm 0.14, 8.1$	0.2	0
				Tuc−Hor (45 ± 4 Myr)						
J00152752−6414545	1.8	$+6.7 \pm 0.3$	+0.5	J001527.62−641455.2	8.70	8.51	8.36	$8.17 \pm 0.25, 5.3$	5.4	0
J00493566−6347416	1.7	$+8.1 \pm 0.3$	+0.2	J004935.79−634742.0	8.33	8.23	8.14	$8.00 \pm 0.18, 6.0$	0.9	0
J01521830−5950168	1.6	$+10.3 \pm 0.3$	+0.1	J015218.43−595016.9	7.96	7.88	7.78	$7.65 \pm 0.09, 11.9$	0.6	0
J02001277−0840516	2.1	$+4.5 \pm 0.4$	−1.0	J020012.84−084052.4	7.77	7.68	7.59	$7.54 \pm 0.14, 7.7$	0.2	0
J02125819−5851182	1.9	$+9.1 \pm 0.8$	+2.1	J021258.28−585118.3	8.31	8.21	8.10	$8.03 \pm 0.15, 7.4$	1.4	0
J02205139−5823411	3.2	$+12.1 \pm 0.6$	+0.5	J022051.50−582341.3	8.67	8.53	8.38	$8.04 \pm 0.16, 6.9$	2.6	1.5
J02474639−5804272	1.8	$+13.1 \pm 0.5$	+0.3	J024746.49−580427.4	8.34	8.24	8.12	$8.09 \pm 0.19, 5.7$	1.8	0
J02564708−6343027	3.6	$+16.7 \pm 4.7$	−3.5	J025647.15−634302.5	8.80	8.63	8.49	$8.25 \pm 0.18, 6.2$	2.8	0.9
J03050976−3725058	1.4	$+14.2 \pm 0.5$	−1.4	J030509.79−372505.8	8.60	8.46	8.33	$8.30 \pm 0.18, 5.9$	3.5	0
J04133314−5231586	2.4	$+18.4 \pm 0.2$	−1.7	J041333.21−523158.5	9.01	8.88	8.74	$8.67 \pm 0.19, 5.7$	2.8	0
J04240094−5512223	2.0	$+19.0 \pm 0.7$	−2.1	J042400.99−551222.2	8.80	8.67	8.51	$8.21 \pm 0.13, 8.2$	3.8	1.3
J04365738−1613065	3.3	$+16.6 \pm 1.9$	+0.1	J043657.44−161306.7	8.14	7.98	7.88	$7.46 \pm 0.14, 7.7$	1.6	0.3
J04440099−6624036	0.0	$+16.0 \pm 0.5$	+0.3	J044401.08−662403.2	8.50	8.47	8.37	$8.13 \pm 0.17, 6.4$	0	0
J05392505−4245211	1.7	$+21.7 \pm 0.2$	−1.2	J053925.08−424521.0	8.47	8.38	8.26	$8.14 \pm 0.19, 5.8$	1.5	0.1
J23124644−5049240	3.9	$+4.1 \pm 1.9$	−1.9	J231246.53−504924.8	8.09	7.90	7.77	$7.74 \pm 0.15, 7.5$	2.7	0
J23285763−6802338	2.3	$+8.0 \pm 1.5$	−1.4	J232857.75−680234.5	8.27	8.16	8.03	$7.96 \pm 0.18, 6.0$	2.0	0
J23474694−6517249	1.0	$+6.1 \pm 0.3$	+0.4	J234747.06−651725.3	8.09	8.02	7.91	$7.96 \pm 0.18, 6.0$	1.0	0
				ABDMG (149^{+51}_{-19} Myr)						
J01034210+4051158	2.6	-10.9 ± 0.4	+0.6	J010342.25+405114.2	8.11	7.94	7.87	$7.62 \pm 0.11, 10.1$	1.7	0.3
J01484087−4830519	6.0	$+21.5 \pm 0.2$	−1.6	J014840.98−483052.3	8.26	8.19	8.08	$8.16 \pm 0.20, 5.4$	0	0
J03472333−0158195	2.5	$+16.0 \pm 1.7$	−1.8	J034723.45−015822.7	6.81	6.66	6.62	$6.45 \pm 0.07, 16.6$	0.2	0
J04522441−1649219	3.0	$+26.7 \pm 1.5$	+0.9	J045224.49−164924.0	6.78	6.58	6.53	$6.39 \pm 0.06, 19.5$	1.6	0
J04571728−0621564	0.5	$+23.4 \pm 0.3$	+0.9	J045717.30−062157.5	8.53	8.51	8.40	$8.08 \pm 0.21, 5.1$	0	1.0
J05254166−0909123	3.5	$+26.3 \pm 0.3$	+2.2	J052541.69−090914.4	7.45	7.31	7.21	$7.06 \pm 0.09, 12.8$	0.7	0
J12383713−2703348	1.5	$+7.8 \pm 1.2$	+0.0	J123837.00−270336.9	7.66	7.57	7.47	$7.30 \pm 0.11, 9.6$	1.0	0.1
J12574030+3513306	4.0	-14.1 ± 1.6	−2.8	J125740.02+351328.7	6.21	6.25	6.31	$6.16 \pm 0.05, 22.7$	0	0
J15244849−4929473	2.0	$+10.3 \pm 0.2$	+2.9	J152448.37−492949.9	7.14	7.02	6.98	$6.99 \pm 0.12, 9.5$	0	0
J16334161−0933116	0.5	-15.0 ± 0.4	+0.0	J163341.57−093313.6	7.46	7.45	7.37	$7.30 \pm 0.13, 8.2$	0	0
J17383964+6114160	0.0	-26.7 ± 0.1	+3.7	J173839.62+611416.5	6.64	6.68	6.64	$6.52 \pm 0.05, 21.2$	0	0
J21464282−8543046	3.5	$+23.5 \pm 0.7$	+1.3	J214644.83−854306.3	7.82	7.65	7.51	$7.25 \pm 0.09, 11.5$	2.9	2.3
J21521039+0537356	2.0	-15.1 ± 0.2	−0.8	J215210.48+053734.4	7.14	7.07	7.00	$6.84 \pm 0.08, 14.0$	0.7	0
J23320018−3917368	3.0	$+11.1 \pm 0.2$	−0.8	J233200.34−391738.9	7.88	7.75	7.63	$7.61 \pm 0.15, 7.4$	1.6	0

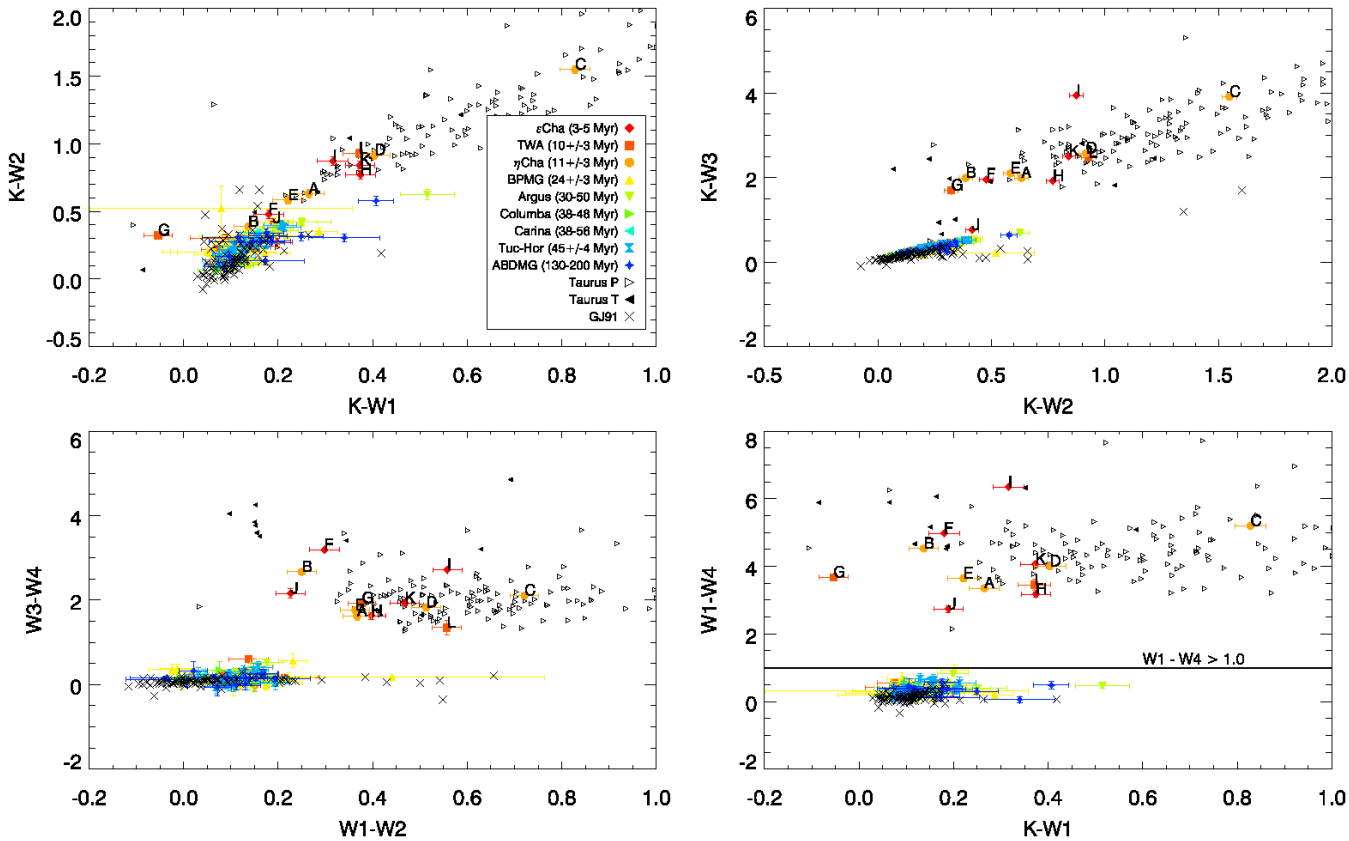

Figure 1. Colour-colour diagrams for the entire sample of M-dwarfs in this analysis with SNR values > 5.0. Taurus P and Taurus T refer to the primordial and transitional disc sample in Esplin, Luhman & Mamajek (2014). Black crosses represent M-type field stars from the Gliese & Jahreiss (1991) catalog. Objects labelled with initials in the $W1-W4$ versus $K-W1$ plot correspond to the 12 targets with $W1-W4>1.0$, listed in Table 3.

amined with the DAOPHOT photometry package in IRAF[2]. All of the detections showed no significant confusion with other sources within the *WISE* point spread function and all bar one showed no evidence of any non-circularity that might betray the presence of multiple components, an extended extragalactic source or cirrus. The exception was target R (see Table 3), which showed marginal evidence for non-circularity, but was our IR-excess source with the lowest detection significance in $W4$. There were also 5 objects with $W1-W4>1.0$, SNR > 5.0, but which were excluded by other criteria described in §2.2 – these are briefly discussed in Appendix A.

4 SED MODELS

For those stars suspected of having an IR excess, SED models were generated to provide a best-fit star plus single-temperature (or two-temperature, if appropriate) disc to the available photometry. BT-Settl model atmospheres were used to simulate photospheres with $T_{\rm eff}>2700$ K (Allard 2014) and the AMES-DUSTY models were used for $T_{\rm eff}\leqslant 2700$ K (Chabrier & Baraffe 2000). All SEDs were fit using atmospheres with [M/H] = 0.0 and $\log g = 4.5$. The flux profiles of the discs were generated from Planck functions. Model fluxes for each photometry point were calculated by integrating the relative spectral response (RSR) curve with the combined stellar and disc flux over the photometric bandwidth (i.e., between λ_1 and λ_2) and dividing this by the integral of the RSR curve.

The photospheric model is constrained using 2*MASS* JHK photometry, assuming that a disc component would contribute negligble flux at these wavelengths, and then this is used as a baseline upon which the disc flux is added. $T_{\rm eff}$ was estimated to the nearest 100 K by comparing spectral-types with the colour-$T_{\rm eff}$ tables in Pecaut & Mamajek (2013), leaving three free parameters to constrain: the disc temperature ($T_{\rm d}$), the surface area of the star and the surface area of the disc. For the cases where we fit a two temperature disc we constrain two disc areas and two disc temperatures. Because the fitted SEDs were calibrated for a source at 10 pc, the flux profiles were multiplied by a normalisation parameter of 10^{η} to characterise the stellar surface area. The value of η was altered until the minimum χ^2_* value was obtained with respect to the JHK photometry. Error bars for η were calculated using a parabolic interpolation of χ^2_* versus η.

[2] IRAF is distributed by the National Optical Astronomy Observatories, which are operated by the Association of Universities for Research in Astronomy, Inc., under cooperative agreement with the National Science Foundation.

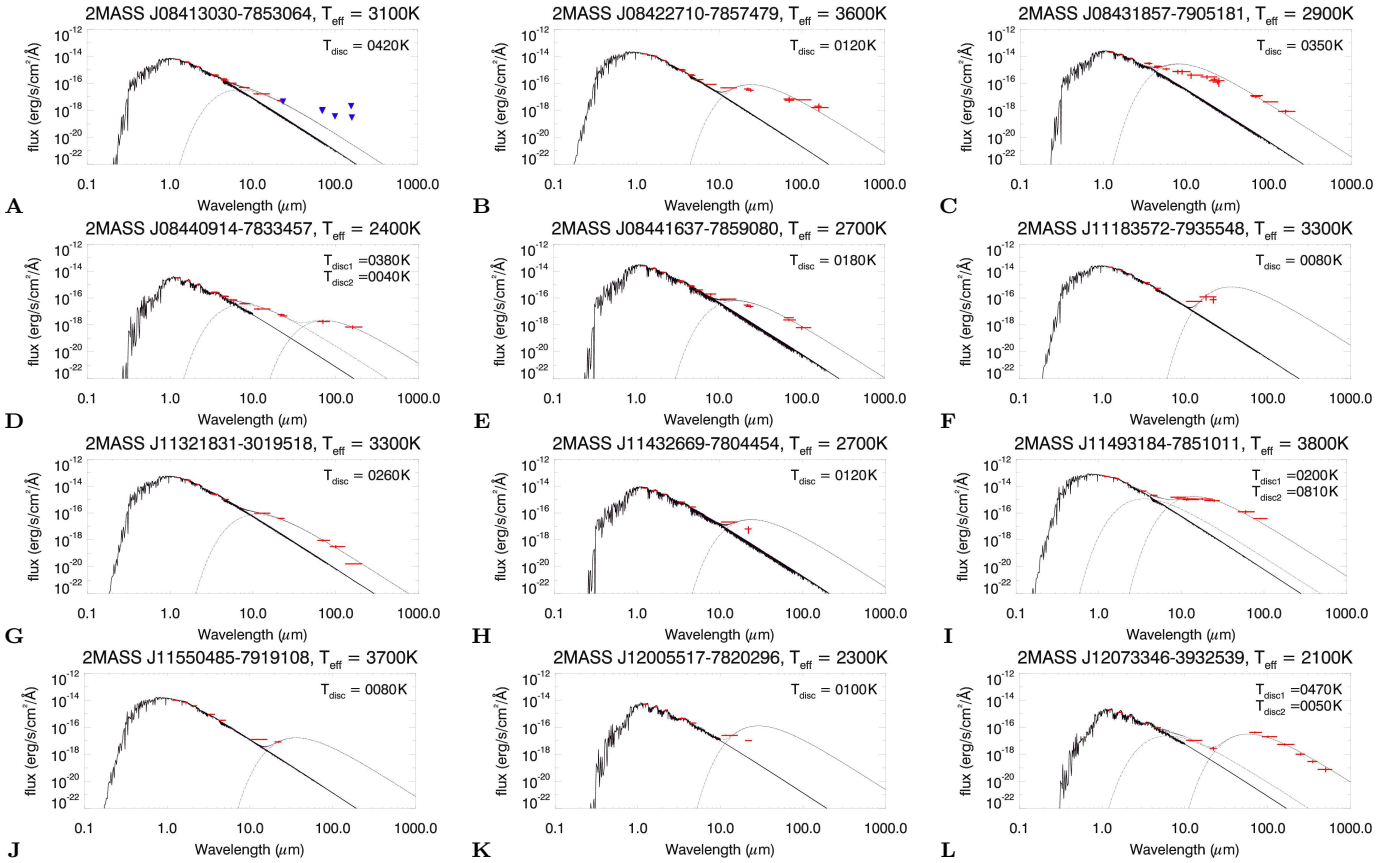

Figure 2. SED models for the 12 objects identified with $W1-W4 > 1.0$. Red symbols represent the flux data and the best-fit stellar SED, single-temperature (or two-temperature) black-body and their sum are overplotted. The fitting parameters for each SED are provided in Table 3. Blue downwards-facing triangles represent values for 3σ upper limits.

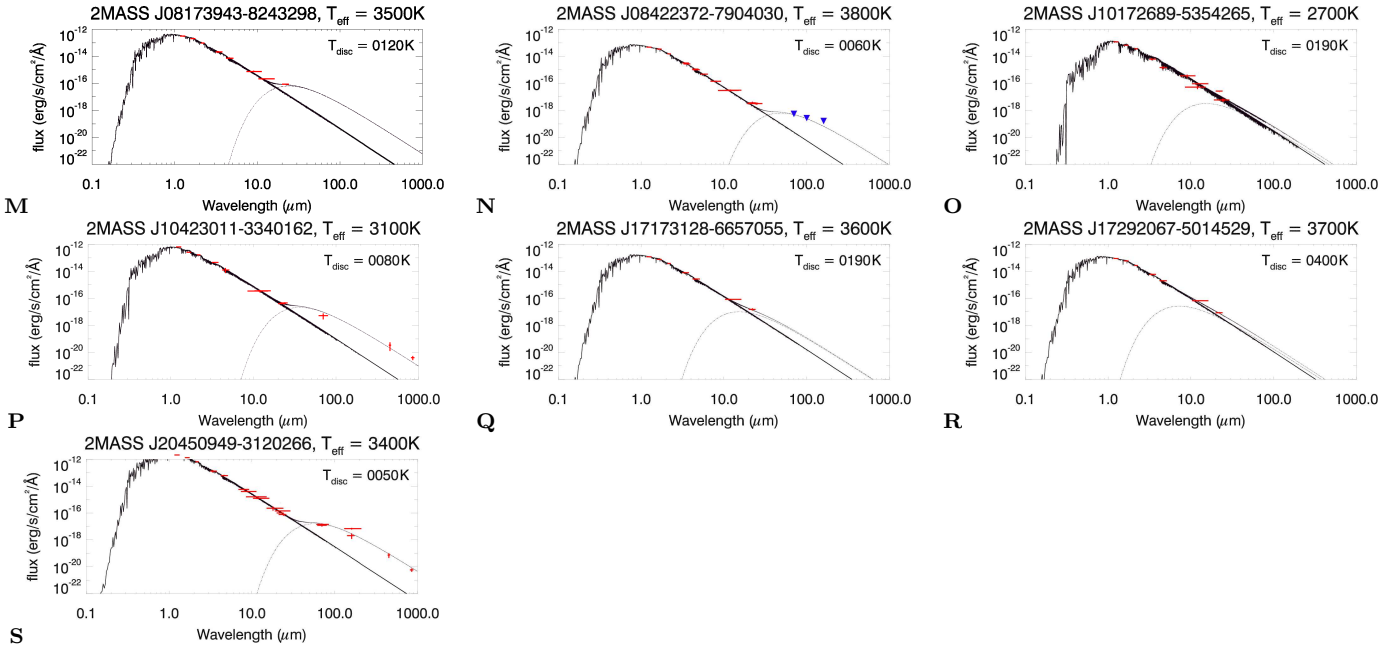

Figure 3. SEDs for objects with $W1-W4 < 1.0$ and $E_{W4} > 3.0$. Only in the cases of TWA 7 (target P) and AU Mic (target S) are data available beyond 25 μm, although EI Cha (target N) is constrained by upper-limits from Herschel PACS 70, 100 and 160 μm.

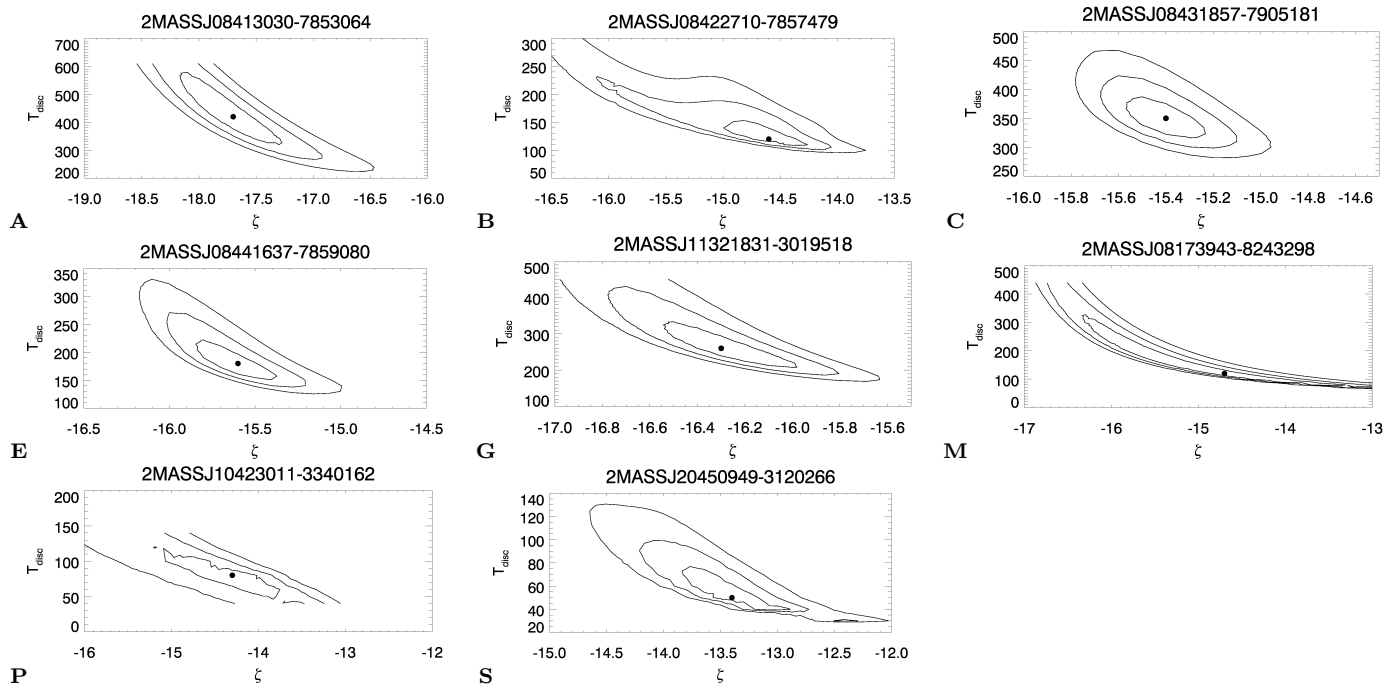

Figure 4. Contour plots indicating the 1, 2 and 3σ errors from simultaneously fitting ζ and $T_{\rm eff}$ in the SED models ($\chi^2_{\rm min}$+ 1, 2 or 3σ, respectively). These were only available for 8 objects because in all other cases there was not enough far-IR data to constrain the disc model.

The η and $T_{\rm eff}$ values are listed in Table 3 and all η errors were ~ 0.01.

A "star plus disc" model was then used and the parameters varied to minimise a chi-squared value labelled as $\chi^2_{\rm d}$ using the best photospheric model, *WISE* photometry and any supplementary IR data available (see Table 4). A single-temperature Planck function was used with the effective disc area and $T_{\rm d}$ as free parameters. Flux upper limits were not included in the chi-square minimisation, however we require that the model flux is less than the upper limits where an upper limit is present. The Planck function normalisation was multiplied by 10^{ζ}, altering ζ in steps of 0.05 and $T_{\rm d}$ in steps of 10 K to provide the lowest $\chi^2_{\rm d}$. We then froze into the model the best-fitting star and single-disc parameters and introduce a second disc using the same ζ and $T_{\rm d}$ steps to obtain a new $\chi^2_{\rm d}$. We use the F-test with two degrees of freedom at the 90 per cent confidence interval to determine whether to use the 1 temperature or 2 temperature model ($\Delta\chi^2 = 9.00$) – for targets D, I and L (see Figure 2) the 2 temperature model is applied.

Uncertainties in ζ and $T_{\rm d}$ were calculated only for single-temperature discs that had IR data either side of the peak of the Planck function (5/12 of the objects with $W1-W4 > 1.0$ and 3/7 of the objects with $W1-W4 < 1.0$). If no IR data were available redward of the Planck function peak then only upper limits to $T_{\rm d}$ could be estimated (see below). In Figure 2, the best-fit star plus disc models are displayed for all 12 objects that had $W1 - W4 > 1.0$ (see §3) and in Figure 4 contour plots are provided for 68, 95 and 99.7 per cent confidence intervals for the simultaneous fits of ζ and $T_{\rm d}$. The maximum/minimum values of ζ and $T_{\rm d}$ which provide 1σ errors in the fit are used as estimates of the error bar on both of these parameters. Figure 3 displays equivalent SED models for the seven objects that have $W1 - W4 < 1.0$ and $E_{W4} > 3.0$ (see §6.2). We cannot provide errors for the two-temperature discs as the fitting process was not performed simultaneously for both discs, but as the aim of this paper is to identify disc candidates, we only require an estimate of the total flux from the disc and are not overly concerned with the detailed parameters for probably over-simplistic disc models.

Table 3 lists the reduced χ^2 values for the photospheric fit and the best disc fit, the corresponding η and ζ values and the corresponding $T_{\rm eff}$ and $T_{\rm d}$ values. The amount of flux from the disc compared to the star ($f_{\rm d}/f_*$, hereafter referred to as the "disc flux fraction") is calculated by integrating the best-fit flux profiles for the disc and star between 0.1 μm and 1.0 mm. In the situation where only *WISE* data were available and the SED did not feature any wavelength points redward of the disc flux peak, the fit was much less constrained and the models more subject to degeneracies. Temperature upper limits (and hence $f_{\rm d}/f_*$ lower limits) for these objects are set at the point where the fit would be excluded with 2σ confidence. There is a strong correlation in the parameter uncertainties. However because lower temperatures goes with higher ζ, the effect on the estimated $f_{\rm d}/f_*$ is not serious.

5 SENSITIVITY LIMITS FOR DETECTING DEBRIS DISCS

A working definition for debris discs is that they have $f_{\rm d}/f_* \leqslant 0.01$ (Lagrange, Backman & Artymowicz 2000). Optically thick primordial discs will generally have much higher values than this. Given that the objects in this

Name/Label 2MASS-	MG	χ^2_*	η	$T_{\rm eff}$ (K)	$N_{\rm IR}$	$\chi^2_{\rm d}$	ζ	$T_{\rm d}$ (K)	$f_{\rm d}/f_*$
				$W1-W4>1.0$					
J08413030−7853064, A	η Cha	0.21	−19.80	3100	8[a]	1.36	-17.7 ± 0.5	420^{+160}_{-100}	$0.043^{+0.037}_{-0.014}$
J08422710−7857479, B	η Cha	2.14	−19.58	3600	14	13.13	$-14.6^{+0.3}_{-0.4}$	120^{+30}_{-10}	$0.118^{+0.093}_{-0.042}$
J08431857−7905181, C	η Cha	16.66	−19.14	2900	17	24.65	-15.4 ± 0.2	350^{+40}_{-30}	$1.170^{+0.448}_{-0.323}$
J08440914−7833457, D	η Cha	0.37	−19.74	2400	11	2.58	−17.5, −13.8	380, 40	0.175
J08441637−7859080, E	η Cha	2.61	−18.98	2700	12	1.95	$-15.4^{+0.1}_{-0.4}$	180^{+130}_{-40}	$0.047^{+0.028}_{-0.016}$
J11183572−7935548, F	ϵ Cha	1.49	−19.36	3300	5*	1.51	−15.1	<250	>0.083
J11321831−3019518, G	TWA	1.60	−19.02	3300	7	0.87	$-16.3^{+0.3}_{-0.2}$	260^{+70}_{-50}	$0.020^{+0.016}_{-0.006}$
J11432669−7804454, H	ϵ Cha	11.02	−19.50	2700	4*	2.78	−17.7	<710	>0.075
J11493184−7851011, I	ϵ Cha	3.58	−19.11	3800	10	6.14	−14.4, −17.6	200, 810	0.455
J11550485−7919108, J	ϵ Cha	25.40	−19.75	3700	4*	6.60	−16.2	<270	>0.013
J12005517−7820296, K	ϵ Cha	0.60	−19.44	2300	4*	2.26	−16.9	<490	>0.094
J12073346−3932539, L	TWA	0.82	−19.69	2100	10	4.39	−18.1, −13.1	470, 50	1.351
				$W1-W4<1.0$ and $E_{W4}>3.0$					
J08173943−8243298, M	BPMG	0.79	−18.19	3500	5	1.73	$-14.7^{+1.4}_{-1.6}$	120^{+210}_{-40}	$0.005^{+0.015}_{-0.002}$
J08422372−7904030, N	η Cha	1.53	−19.14	3800	10*[b]	2.71	−15.2	<60	$>4\times10^{-4}$
J10172689−5354265, O	BPMG	0.53	−18.32	2700	8*	16.50	−17.0	<380	$>6\times10^{-3}$
J10423011−3340162, P	TWA	0.54	−17.85	3100	9	4.64	$-14.3^{+0.5}_{-0.8}$	80^{+40}_{-30}	$16^{+5}_{-6}\times10^{-4}$
J17173128−6657055, Q	BPMG	2.83	−18.69	3600	4*	0.18	−16.5	<380	$>1.1\times10^{-3}$
J17292067−5014529, R	BPMG	0.20	−18.86	3700	4*	0.41	−17.7	<590	$>1.2\times10^{-4}$
J20450949−3120266, S	BPMG	4.58	−17.38	3400	16	6.67	$-13.4^{+0.5}_{-0.4}$	50^{+30}_{-10}	$4^{+6}_{-3}\times10^{-4}$

Table 3. Best-fit parameters to SED models for the sample of objects with evidence of IR excess. The number of flux points at wavelengths longer than K are provided in column 3. *No data available to constrain the disc at wavelengths longer than the peak wavelength of the black-body fit — 2σ upper/lower limits are provided for $T_{\rm d}$ and $f_{\rm d}$ for these (see §5). Error bars for the η values are ~ 0.01. **Two temperature models are fitted for targets D, I and L.** [a] **3σ upper-limits from *MIPS* 24, 70 and 160 μm and Herschel 70, 100 and 160 μm; these are used only as a constraint in the SED modelling such that model fluxes at these wavelengths must lie below the upper limits.** [b] **3σ upper-limits from Herschel 70, 100 and 160 μm.**

work are relatively faint M-dwarfs, there will be a limiting $W1-W4$ for which $f_{\rm d}/f_* \leqslant 0.01$.

To explore the relationship between $f_{\rm d}/f_*$ and $W1-W4$, a simulation was made to artifically increase the $W4$ flux from a disc-less M-dwarf star until $f_{\rm d}/f_* = 0.01$. The disc-less stars used in the simulation are 2MASSJ05531299−4505119 (M0.5V, ABDMG), BD+36 2322 (M4V, ABDMG) and DEN 1048−3956 (M8.5, field brown dwarf – see Avenhaus, Schmid & Meyer 2012). Photospheres were modelled using the same procedure described in §4. The disc temperature was fixed at either 100 K or 300 K and the threshold $W4$ magnitude and disc area are outputs from the model.

For comparison, the same simulation was carried out for an F5, a G3 and a K7 star (HIP 19183, HIP 113579 and HIP 31878, respectively, all members of the ABDMG). The simulations show (see Figure 5), for the assumed disc temperatures chosen, that $W1-W4>1.0$ corresponds to $f_{\rm d}/f_* > 10^{-3}$ for K- to mid-M-dwarfs (and $>3\times10^{-4}$ for F- and G-dwarfs). Sensitivity to (debris) discs with less IR flux than this, using $W1-W4$, is compromised because smaller $W4$ excesses become indistinguishable from the scatter in $W1-W4$ values seen in disc-less field stars.

The $W1-W4$ colour at which $f_{\rm d}/f_* \geqslant 0.01$ is ≈ 2.5 for early to mid-M spectral-types and ≈ 2.2 for late M-dwarfs. Given that M8/9 represents the faintest object in the MG sample, this suggests that debris discs will have $W1-W4$ values somewhere between these upper limits and the $W1-W4$ values of disc-less field stars. Primordial discs should have $W1-W4>2.2$. For F and G stars the sensitivity improves, and debris disc objects should have $W1-W4<$

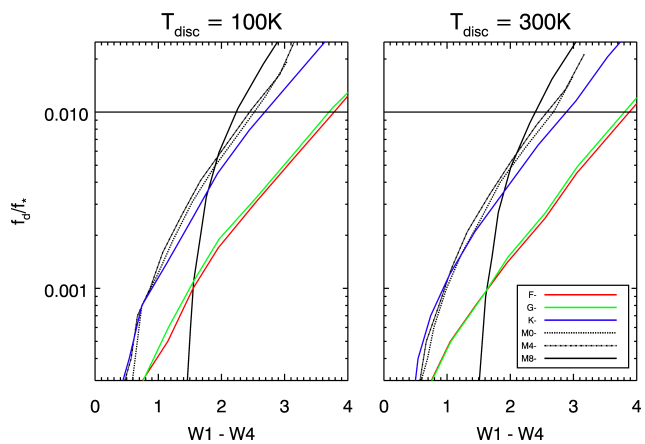

Figure 5. Sensitivity limits for detecting debris discs in stars of various spectral types, with assumed disc temperatures of 100 K (left) and 300 K (right).

3.7. Observations of K stars are only slightly more sensitive than M-dwarfs and debris discs should have $W1-W4<2.8$. There were only small differences of $W1-W4\sim0.1$ mag in the results depending on whether a disc temperature of 100 K or 300 K was adopted. These simple models do not take into account disc gaps or disc orientation, which will be an additional source of scatter.

Figure 6 is an alternative way of looking at this sensitivity to debris discs, showing the relationship between

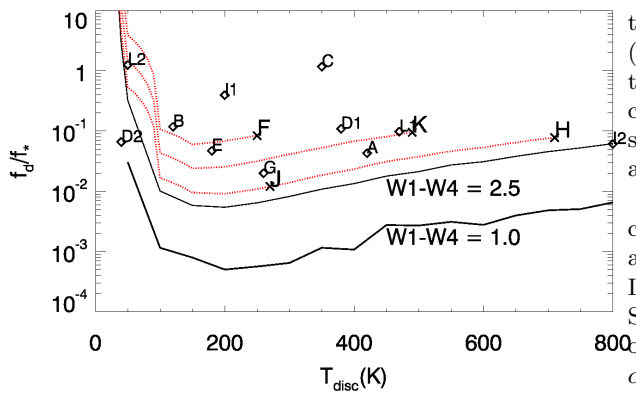

Figure 6. Diagram showing the expected relationship between $f_{\rm d}/f_*$ and disc temperature at a given $W1-W4$ for an M0 star. For comparison with Figure 5 we have plotted the $f_{\rm d}/f_*$ vs $T_{\rm d}$ at constant $W1-W4 = 1.0$ and 2.5. Diamond symbols indicate our 6 objects which have a measured $T_{\rm d}$ and $f_{\rm d}/f_*$. For the other 6 objects only with an upper limit to the disc temperature we plot lines of constant $W1-W4$ which terminate at their 2-sigma $T_{\rm d}$ upper limits, as described in §4. We note that none of these objects could have $f_{\rm d}/f_* < 0.01$. For targets D, I and L with two-temperature fits we split the flux from each disc into their two components and label them as '1' and '2'.

disc temperature and $f_{\rm d}/f_*$ at a fixed M0 spectral-type for $W1-W4 = 1.0$ and 2.5 respectively. We find that debris discs with $f_{\rm d}/f_* < 0.01$ must have $T_{\rm d} > 70\,$K if they are to have $W1-W4 > 1.0$. The debris disk threshold of $f_{\rm d}/f_* < 0.01$ corresponds to $W1-W4 < 2.5$ for $100 < T_{\rm d} < 300\,$K and $W1-W4 \lesssim 2.0$ for $300 < T_{\rm d} < 500\,$K.

6 NATURE OF THE IR EXCESS

6.1 Disc criteria

This section focuses on objects that have $W1-W4 > 1.0$. In §6.2 objects with $W1-W4 < 1.0$ and $E_{W4} > 3.0$ are discussed. A variety of indicators have been used in the literature to try to separate primordial, transitional and debris discs and we examine these with our sample. The final disc designation for each target is listed in Table 4.

Figure 1 shows four separate colour-colour diagrams for the entire sample used in this analysis. Large $K-W1$ and $K-W2$ colours are indicative of large amounts of near-IR flux, consistent with what is expected from primordial discs. In Table 4 we assign a disc type of either 'P' (primordial) or 'T' (transitional) based on an object's position (see Figure 1) in the $K-W2$ versus $K-W1$ (top-left), $K-W3$ versus $K-W2$ (top-right) and $W3-W4$ versus $W1-W2$ (bottom-left) diagrams compared with the distribution of primordial and transitional discs observed in Taurus. The bottom-right panel in Figure 1 ($W1-W4$ versus $K-W1$) is the most effective way of separating debris discs from primordial discs, given only $2MASS$ and $WISE$ data, as it can potentially probe both hot discs ($K-W1$) and cooler discs ($W1-W4$). Figure 1 shows that both primordial and transitional discs in Taurus have colours of $3 < W1-W4 < 6$, which is consistent with the simulations in §5. Overall it appears that transitional discs have slightly larger $W1-W4$ values (~ 4.5 to 6.0) although not enough to strongly distinguish them from primordial discs. Choosing a disc type based on colour-colour diagrams is ambiguous, although the evidence suggests the majority of our targets with $W1-W4 > 1.0$ are primordial/transitional.

We expect debris discs to be class III sources. If they are class II sources then it is likely that any NIR excess is from a primordial disc. Because discs contribute large amounts of IR flux compared to the star, the flux gradient observed in SEDs is shallower than for objects without discs. The slope of the SED at IR wavelengths is characterised by α, where $\alpha = {\rm d}\log\lambda F_\lambda/{\rm d}\log\lambda$. In identifying the disc frequencies amongst brown-dwarfs in the Upper Scorpius OB association Riaz et al. (2012) suggest that objects with $\alpha_{K-W3} \geqslant -0.2$, $-1.8 < \alpha_{K-W3} < -0.2$ and $\alpha_{K-W3} \leqslant -2.0$ correspond to class I/II/III sources, respectively. This method was calibrated for objects as early as M3.5 and should be applicable to most M-dwarfs in this work. There is an overlap of class II/III sources between $-2.0 < \alpha < -1.8$. Should an object have $-2.0 < \alpha_{K-W3} < -1.8$ it is assumed to be class III.

We choose the disc flux fractions as the most important indicator of disc type and this indicator has been recommended in several previous works (Lagrange, Backman & Artymowicz 2000; Wyatt 2008; Matthews et al. 2014). We have values or upper limits which make a decision between debris disc and transitional/primordial disc rather clear. Debris discs generally have $f_{\rm d}/f_* < 0.01$, whereas Cieza et al. (2012) estimate primordial discs to have $f_{\rm d}/f_* \gtrsim 0.1$. In this work objects with $f_{\rm d}/f_* > 0.1$ are classed as primordial, $0.01 < f_{\rm d}/f_* < 0.1$ are either primordial or transitional and $f_{\rm d}/f_* < 10^{-2}$ are debris discs. In the case of target B, the most probable disc-type based on $f_{\rm d}/f_*$ is primordial, however, this is less than 1 error bar from the primordial and primordial/transitional boundary and we flag this object accordingly in Table 4. If we were to only use the hotter component in the two-temperature models our disc classification would remain the same. The addition of an extra, cooler disc increases our $f_{\rm d}/f_*$, but in no cases is this by enough to change the type of disc we infer.

Figure 6 illustrates this test for both stars with estimated disc temperatures and for those with upper limits to disc temperatures. For the latter, their $W1-W4$ colour defines a locus in the $f_{\rm d}/f_*$ versus $T_{\rm d}$ diagram which terminates at their 2σ disc temperature upper limits. Assuming that all 12 of our targets with $W1-W4 > 1.0$ are similar to M0 stars, we find that none of them have $f_{\rm d}/f_* < 0.01$, and this remains true even when a more precise spectral-type is chosen (see Table 3). For targets that only have upper limits for $f_{\rm d}/f_*$ we report the disc type as the type corresponding to the upper limit, however, we place in parenthesis other possible disc types. Five excesses appear to be due to primordial discs, whilst the remainder are either primordial or transitional discs.

In Table 4 we provide the results of our deliberations of disc type using each method described in this section. The $f_{\rm d}/f_*$ classification assumes primacy, followed by consideration of the other indicators where this is ambiguous. The final totals are 8 primordial discs, 4 transitional discs and no debris discs.

Label/Common identifier	$W1-W4$	Excess	α	$f_{\rm d}/f_*$	Final	Additional fluxes ($\times10^{-15}$ erg/s/cm^2/Å)
			$W1-W4>1.0$			
A, ES Cha	3.39	PPP(P)	II	T/P	P	0.41 (3.6) 0.21 (4.5) 0.10 (5.8) 0.05 (8) < 0.004 (M24) < 0.001 (M70) < 0.0009 (H70) < 0.0004 (H100) < 0.002 (M160) < 0.0003 (H160)[a]
B, EK Cha	4.53	TTT(P/T)	III	P(P/T?)	P?	0.96 (3.6) 0.43 (4.5) 0.19 (5.8) 0.08 (8) 0.03 (M24) 0.006 (M70) 0.007 (H70) 0.006 (H100) 0.002 (M160) 0.002 (H160)[a]
C, ET Cha	5.15	PPP(P)	II	P	P	2.93 (3.6) 1.87 (4.5) 1.15 (5.8) 0.76 (8) 0.74 (9) 0.30 (18) 0.12 (M24) 0.16 (25) 0.01 (M70) 0.01 (H70) 0.004 (H100) 0.0009 (M160) 0.0008 (H160)[a]
D, RECX 16	3.94	PPP(P)	II	P	P	0.26 (3.6) 0.14 (4.5) 0.07 (5.8) 0.04 (8) 0.004 (M24) 0.002 (H70) 0.0007 (H160)[a]
E, EN Cha	3.61	TPP(P/T)	II	T/P	T	1.67 (3.6) 0.82 (4.5) 0.40 (5.8) 0.20 (8) 0.02 (M24) 0.003 (M70) 0.002 (H70) 0.0006 (H100)[a]
F, ϵ Cha 13	4.95	TTT(P/T)	III	T/P(P?)	T?	0.12 (18)
G, TWA 30	3.64	TPT(P/T)	III	T/P	T	0.0009 (H70) 0.0003 (H100) 0.00002 (H160)[b]
H, ϵ Cha 17	3.12	PPP(P)	III	T/P(P?)	P?	
I, ϵ Cha 1	6.38	PPP(P/T)	II	P	P	1.50 (9) 1.13 (12) 1.09 (18) 0.84 (25) 0.12 (60) 0.04 (90)
J, T Cha B	3.03	TTP(P/T)	III	T/P(P?)	T?	
K, ϵ Cha 10	4.01	PPP(P)	II	T/P(P?)	P?	
L, 2M 1207	3.53	PPP(P)	II	P	P	0.04 (H70) 0.02 (H100) 0.005 (H160) 0.001 (250) 0.0003 (350) 0.00008 (500)[c]
			$W1-W4<1.0$ and $E_{W4}>3.0$			
M, 2MASS J08173843−8243298	0.43	T/D	III	D(P/T?)	D?	0.76 (9)
N, EI Cha	0.75	T/D	III	D(T?P?)	D?	2.75 (3.6) 1.14 (4.5) 0.47 (5.8) 0.14 (8.0) 0.03 (12) 0.003 (M24) 0.003 (25) < 0.0006 (H70) < 0.0003 (H100) < 0.0002 (H160)[a]
O, TWA 22AB	0.26	T/D	III	D(T?P?)	D?	0.36 (9) 0.053 (12) 0.006 (M24) 0.006 (25)
P, TWA 7	0.79	T/D	III	D	D	0.040 (12) 0.046 (M24) 0.005 (M70) 0.00003 (450) 0.000004 (850)[d]
Q, HD 155555C	0.59	T/D	III	D(T?P?)	D?	
R, GSC 08350−01924	0.23	T/D	III	D(T?P?)	D?	
S, AU Mic	0.36	T/D	III	D	D	1.39 (9) 1.59 (12) 0.22 (18) 0.076 (M24) 0.14 (25) 0.01 (M70) 0.01 (H70) 0.002 (M160) 0.007 (H160)[e]

Table 4. Disc types derived from various methods described in this work. The labels in column 1 refer to the 2MASS sources in Table 3. The excess column is an approximation of the disc-type based on the $K-W2$ vs $K-W1$, $K-W3$ vs $K-W2$, $W3-W4$ vs $W1-W2$ and $W1-W4$ vs $K-W1$ (in parentheses) colour-colour diagrams (respectively) of Figure 1. For objects with $W1-W4<1.0$, only the $W1-W4$ vs $K-W1$ disc designation is prescribed. The entries in column 4 categorise an object as a class II or class III source based on the α slopes calculated in §3. **The disc types derived from disc flux fractions are provided in column 5 where designations in parentheses are alternative possible disc types as described in §6.1**. The final derived disc type is given in column 6. P = primordial disc, T = transitional disc, D = debris disc. The final column lists any additional fluxes where values in parentheses are the wavelengths (in μm) for each data point: 3.6, 4.5, 5.8 and 8 are from *IRAC*; 12, 25, 60 and 100 are from *IRAS*; M24, M70 and M160 are from *MIPS*; **H70, H100 and H160 are from** *Herschel PACS*; **250, 350 and 500 are from** *Herschel SPIRE*; **450 and 850 are from** *SCUBA*2 **and 9, 18 and 90 are from** *AKARI*. **Additional fluxes prefixed with '<' are 3σ upper limits. Fluxes from** *Herschel* **or** *SCUBA*2 **provided in: a) ?; b) ?; c) Riaz et al. (2012); d) ?; e) ?**.

6.2 Other disc candidates identified with $W4$ excess

In this section we analyse the 7 objects with $W1-W4<1.0$ and $E_{W4}>3.0$ that are listed towards the bottom of Table 4. There is one member of η Cha (target N=EI Cha), one TWA member (target P=TWA 7) and five BPMG members (targets M=2MASSJ08173843−8243298, hereafter 2MJ0817; O=TWA 22AB; Q=HD 155555C; R=2MASSJ17292067−5014529, hereafter 2MJ1729 and S=AU Mic).

SEDs were modelled for these seven objects using the same procedure described in §4 and are displayed in Figure 3, with results listed in Table 3. Only three of these objects had estimated values of $T_{\rm d}$ and $f_{\rm d}/f_*$, all of which were less than 0.01 (2M J0817, TWA 7 and AU Mic, see Cotten & Song 2016). For 2M J0817, the flux fraction is within one error bar of 0.01, the boundary between debris

and primordial/transitional discs. AU Mic and TWA 7 are already well-known to have a debris disc that has been imaged in scattered light (Kalas 2004; Choquet et al. 2016).

TWA 22AB, 2M J1729 and HD 155555C did not have sufficient data at far-IR wavelengths to constrain a disc fit and no information on their disc type or $f_{\rm d}/f_*$ could be found in previous works, however **?** claim a null detection of IR excess for HD 155555C based on mid-IR spectroscopic measurements between $8-13\,\mu$m. Disc temperature upper limits of 80, 120 and 180 K, and corresponding $f_{\rm d}/f_*$ lower limits of 6.0×10^{-3}, 1.1×10^{-3} and 1.2×10^{-4}, respectively, were estimated, so these were classed here as candidate debris discs which require further observation. EI Cha also had unconstrained disc parameters in this work; EI Cha has previously been flagged as a possible debris disk source with $f_{\rm d}/f_*=3\times10^{-5}$ (based on far-IR Herschel photometry) by Gautier et al. (2008), however in our work we only calculate a lower-limit to $f_{\rm d}/f_*$ because the Herschel data for EI Cha are upper limits.

In summary, this set of seven candidates, with small but significant $W4$ excesses, consists of three "recovered" objects whose status as debris disc objects was already known or suspected, together with a new probable debris disc source (2M J0817) and three new candidate debris disc sources (targets TWA 22AB, HD 155555C and 2M J1729) that are all likely members of the BPMG.

6.3 Comparison with the literature

Many of the 19 stars we have identified as harbouring discs have been previously identified or studied. Appendix B gives a star-by-star comparison with literature values and classifications. There are some differences between our estimates of $f_{\rm d}/f_*$ and those in the literature, but not by enough to change our disc classifications. For the 12 objects with $W1-W4>1.0$, in all but two cases there is broad agreement and agreement on the nature of the disc: for ϵ Cha 17 and 2M J1207 (targets H and L) we find primordial discs whereas in the literature these were reported as transitional and debris discs, respectively (Manoj et al. 2011 and Riaz & Gizis 2012). Four of the seven objects with $W1-W4<1.0$, but significant $W4$ excess have been reported in previous work as either confirmed debris discs or debris disc candidates, which is in broad agreement with our classification scheme.

7 DISCUSSION

7.1 Did we find *any* new debris discs?

We have identified IR ($22\,\mu$m) excesses from 19/100 M-dwarfs that are likely MG members. These excesses are bimodal in nature – 12 sources have $W1-W4>3$, which simple disc models suggest corresponds to $f_{\rm d}/f_*>0.02$ for these spectral-types; 7 sources have $W1-W4<1$ and although we are unable to adequately constrain the disc temperatures, it is likely that these have $f_{\rm d}/f_*\lesssim3\times10^{-3}$. The former objects are all almost certainly primordial, gas-rich discs, although some may have transitional inner holes as recorded by our classifications in Table 5. The latter do not exhibit excesses at shorter wavelengths or signs of accretion activity and should be regarded as debris disc *candidates*, although some confidence in our methods is drawn from the fact that these include 2 objects with previously known debris discs that have been imaged in scattered light and another object identified as a debris disc in other studies. The four remaining candidates need additional sensitive measurements at mid- and far-IR wavelengths in order to confirm their nature.

MG Name	$N_{\rm sample}$	P	T	D
ϵ Cha	8	3	2	0
TWA	11	1	1	1
η Cha	8	4	1	1
BPMG	28	0	0	5
Total	55	8	4	7

Table 5. The number of primordial (P), transitional (T) or debris (D) discs for each MG that contains at least one type of disc. $N_{\rm sample}$ is the number of M-dwarfs in the MG which satisfy all criteria described in §2.

Table 5 provides the number of primordial, transitional or debris discs for each MG containing at least one disc. All of the IR excess objects were found in MGs with age <30 Myr. The total fraction of M-dwarf MG members with debris discs identified in this work is 7/100. Given that identification of debris discs for objects with $W1-W4<1$ is incomplete then this fraction is of course a lower limit and likely to be age-dependent. No debris disc candidates are found with $1.0<W1-W4<3.0$, implying that <3 per cent of young M-dwarfs have very dusty debris discs with $f_{\rm d}/f_*\gtrsim10^{-3}$.

7.2 Evidence for debris disc evolution in M-dwarfs?

All of the discs we have found, primordial, transitional or debris, are in MGs at the age of BPMG (24 ± 4 Myr) or younger. This is consistent with the claimed lifetimes of primordial discs in M-dwarfs (2–3 Myr, Williams & Cieza 2011), but may also be evidence for a decline of debris disc frequency with age. Dividing the sample into MGs younger and older than 30 Myr, there are 7/55 debris disc candidates in the younger group and 0/45 in the older group. This corresponds to debris disc frequencies of 12 ± 5 per cent in the younger group and <7 per cent (at 95 per cent confidence) in the older group. Assuming that the younger and older samples were observed with similar sensitivities, then a 2×2 chi-squared contingency test suggests a difference in these frequencies at 98.5 per cent confidence.

Gautier et al. (2007) found no evidence for debris discs in a sample of 62 field M dwarfs that were estimated to be older than 1 Gyr. Lestrade et al. (2009) identified only one object (GJ842.2) from a sample of 19 M-dwarfs younger than 200 Myr as having a cold debris disc based on sub-mm observations, deriving a debris disc frequency of $5.3^{+10.5}_{-5.0}$ per cent. Following a deep *Spitzer MIPS* survey, Forbrich et al. (2008) found evidence for debris discs with a $24\,\mu$m excess for 11 M-dwarfs in NGC 2547 (age 35 ± 3 Myr, Jeffries & Oliveira 2005), providing a lower limit to the debris disc frequency of 4.9 per cent. Our measurement of a debris disc frequency (for MG members with ages of 30–

150 Myr) of < 7 per cent is consistent with all of this previous work.

7.3 Do M-dwarfs dissipate their discs faster than solar-type stars?

There have been suggestions in the literature that M-dwarfs may disperse their debris disks more rapidly than higher mass stars, due to drag caused by stronger stellar winds (Wood et al. 2002; Plavchan, Jura & Lipscy 2005), by earlier photoevaporation due to the stonger EUV and FUV radiation fields (Galván-Madrid et al. 2014) or by the stripping of planetestimals from less massive M-dwarfs due to stellar encounters (Lestrade et al. 2009), but these arguments also depend on a straightforward linear scaling between disc mass and stellar mass. The empirical situation is far from clear due to the small number of identified M-dwarf debris discs and the difficulties of comparing samples with threshold sensitivities that vary with brightness and spectral-type.

A straightforward comparison between FGK-stars in MGs and the M-dwarfs studied in this work is difficult because of small numbers and whilst *WISE* can detect debris discs amongst FGK-dwarfs with $f_{\rm d}/f_* > 3 \times 10^{-4}$ (corresponding to $W1 - W4 \geqslant 1.0$ – see Figure 5), data of the same quality is only capable of detecting M-dwarf debris discs if they have $f_{\rm d}/f_* > 10^{-3}$. The only comparable study was performed by Moór et al. (2016) who surveyed 29 FGK members of MGs with ages of 20–50 Myr, finding 6 debris discs with $10^{-4} < f_{\rm d}/f_* < 10^{-3}$. The frequency of discs in the older FGK stars with age 30–50 Myr was 5/25. A 2×2 chi-squared contingency test suggests that this is incompatible (at > 99 per cent confidence) with the lack of debris discs we have found in M-dwarfs at similar ages, however it could be that the survey for FGK debris discs is more sensitive and thus more complete, with several M-dwarf debris discs with $10^{-4} < f_{\rm d}/f_* < 10^{-3}$ awaiting discovery.

It has also been suggested that although dust may be dispersed more rapidly around M-dwarfs there could be a delay in the production of dust from planetestimal collisions with respect to higher mass stars, with the time of maximum dust visibility $t_{\rm max} \propto M_*^{-1}$ (Kenyon & Bromley 2008). Empirically, the strength of debris disc emission and the debris disc frequency both appear to peak at ∼20–30 Myr in FGK stars but occur earlier at 10–20 Myr for A/B-type stars (Currie et al. 2008; Hernández et al. 2009; Smith & Jeffries 2012). There is no evidence from our survey that this trend continues towards lower masses – our data would suggest that any peak in dust visibility for M-dwarfs occurs at $\leqslant 30$ Myr.

8 SUMMARY

We have performed a survey using 2*MASS* and *WISE* for discs around a sample of 100 candidate M-dwarf members of young MGs (with ages of 5–150 Myr). Potential discs were identified on the basis of significant $W1 - W4$ excesses and their nature investigated using a variety of diagnostics including simple models for the SEDs and longer wavelength data where available.

Tests of the sensitivity of *WISE* data to dust discs suggest that debris discs should have been readily identified around M-dwarfs if $W1 - W4 > 1.0$, corresponding to a disc flux fraction $f_{\rm d}/f_* > 10^{-3}$. For stars with $W1 - W4 < 1.0$, significant excess can be detectable, but becomes harder to separate from the photospheres of (presumed disc-less) M-dwarf field stars. The main results of our search are:

1. We found 12 objects with clear IR excesses and $W1 - W4 > 3.0$, all were younger than 30 Myr, all have $f_{\rm d}/f_* > 0.02$ and all have SEDs consistent with primordial discs or transitional discs with inner holes.

2. No M-dwarfs were found with $1.0 < W1 - W4 < 3.0$, indicating that < 3 per cent (at 95 per cent confidence) of young M-dwarfs have very dusty debris discs with $f_{\rm d}/f_* \gtrsim 10^{-3}$.

3. Seven objects were identified with $W1 - W4 < 1.0$ but with a significant $W4$ excess over that expected from the photosphere, corresponding to $f_{\rm d}/f_* \lesssim 3 \times 10^{-3}$, although the disc flux fractions and disc temperatures are poorly constrained. These IR excesses are assumed to be due to debris discs and all these stars are younger than 30 Myr. Three of the debris discs have been previously identified in the literature and in two cases the discs have been imaged in scattered light. The four other sources are new debris disc candidates and all are candidate members of the BPMG.

4. The frequency of debris discs in young M-dwarfs with age < 30 Myr is at least 13 ± 5 per cent, but this falls to < 7 per cent in older MG M-dwarfs at equivalent observational sensitivity. This provides evidence for some evolution of debris disc properties and argues against the peak of debris disc activity occurring later in lower-mass stars.

9 ACKNOWLEDGEMENTS

ASB acknowledges the financial support from the United Kingdom Science and Technology Funding Council (STFC) and the Consejo Nacional de Ciencia y Tecnología (México). RDJ acknowledges financial support from the STFC. This publication makes use of data products from the Wide-field Infrared Survey Explorer, which is a joint project of the University of California, Los Angeles, and the Jet Propulsion Laboratory/California Institute of Technology, funded by the National Aeronautics and Space Administration. This research has made use of the NASA/IPAC Infrared Science Archive, which is operated by the Jet Propulsion Laboratory, California Institute of Technology, under contract with the National Aeronautics and Space Administration. This work is based [in part] on observations made with the Spitzer Space Telescope, which is operated by the Jet Propulsion Laboratory, California Institute of Technology under a contract with NASA. This publication makes use of data products from the Two Micron All Sky Survey, which is a joint project of the University of Massachusetts and the Infrared Processing and Analysis Center/California Institute of Technology, funded by the National Aeronautics and Space Administration and the National Science Foundation. This research is based on observations with AKARI, a JAXA project with the participation of ESA. This research has made use of the SIMBAD database, operated at CDS, Strasbourg, France. We thank an anonymous referee for their comments and suggestions which improved this manuscript.

References

Allard F., 2014, in IAU Symposium, Vol. 299, IAU Symposium, Booth M., Matthews B. C., Graham J. R., eds., pp. 271–272

Augereau J.-C., Beust H., 2006, A&A, 455, 987

Avenhaus H., Schmid H. M., Meyer M. R., 2012, A&A, 548, A105

Backman D. E., Paresce F., 1993, in Protostars and Planets III, Levy E. H., Lunine J. I., eds., pp. 1253–1304

Barman T. S., Macintosh B., Konopacky Q. M., Marois C., 2011, ApJ, Letters to the Editor, 735, L39

Barrado y Navascués D., Stauffer J. R., Song I., Caillault J.-P., 1999, ApJ, Letters to the Editor, 520, L123

Bell C. P. M., Mamajek E. E., Naylor T., 2015, MNRAS, 454, 593

Binks A. S., Jeffries R. D., 2014, MNRAS, 438, L11

Binks A. S., Jeffries R. D., 2016, MNRAS, 455, 3345

Binks A. S., Jeffries R. D., Maxted P. F. L., 2015, MNRAS, 452, 173

Chabrier G., Baraffe I., 2000, Ann, Rev A&A, 38, 337

Choquet É. et al., 2016, ApJ, Letters to the Editor, 817, L2

Cieza L. A. et al., 2013, ApJ, 762, 100

Cieza L. A., Schreiber M. R., Romero G. A., Williams J. P., Rebassa-Mansergas A., Merín B., 2012, ApJ, 750, 157

Cohen M., Wheaton W. A., Megeath S. T., 2003, AJ, 126, 1090

Cotten T. H., Song I., 2016, ApJ, Supplement Series, 225, 15

Currie T., Kenyon S. J., Balog Z., Rieke G., Bragg A., Bromley B., 2008, ApJ, 672, 558

Currie T., Sicilia-Aguilar A., 2011, ApJ, 732, 24

Cutri R. M. et al., 2003, 2MASS All Sky Catalog of point sources.

De Silva G. M., D'Orazi V., Melo C., Torres C. A. O., Gieles M., Quast G. R., Sterzik M., 2013, MNRAS, 431, 1005

Ducourant C., Teixeira R., Galli P. A. B., Le Campion J. F., Krone-Martins A., Zuckerman B., Chauvin G., Song I., 2014, A&A, 563, A121

Elliott P., Bayo A., Melo C. H. F., Torres C. A. O., Sterzik M. F., Quast G. R., Montes D., Brahm R., 2016, A&A, 590, A13

Esplin T. L., Luhman K. L., Mamajek E. E., 2014, ApJ, 784, 126

Fang M., van Boekel R., Bouwman J., Henning T., Lawson W. A., Sicilia-Aguilar A., 2013, A&A, 549, A15

Forbrich J., Lada C. J., Muench A. A., Teixeira P. S., 2008, ApJ, 687, 1107

Gagné J., Lafrenière D., Doyon R., Malo L., Artigau É., 2014, ArXiv e-prints

Gagné J., Lafrenière D., Doyon R., Malo L., Artigau É., 2015, ApJ, 798, 73

Galván-Madrid R. et al., 2014, A&A, 570, L9

Gautier, III T. N., Rebull L. M., Stapelfeldt K. R., Mainzer A., 2008, ApJ, 683, 813

Gautier, III T. N. et al., 2007, ApJ, 667, 527

Gliese W., Jahreiss H., 1991, NASA STI/Recon Technical Report A, 92, 33932

Haisch, Jr. K. E., Lada E. A., Lada C. J., 2001, ApJ, Letters to the Editor, 553, L153

Helou G., Walker D. W., eds., 1988, Infrared astronomical satellite (IRAS) catalogs and atlases. Volume 7: The small scale structure catalog, Helou G., Walker D. W., eds., Vol. 7

Hernández J., Calvet N., Hartmann L., Muzerolle J., Gutermuth R., Stauffer J., 2009, ApJ, 707, 705

Hernández J., Hartmann L., Calvet N., Jeffries R. D., Gutermuth R., Muzerolle J., Stauffer J., 2008, ApJ, 686, 1195

Huélamo N., Lacour S., Tuthill P., Ireland M., Kraus A., Chauvin G., 2011, A&A, 528, L7

Jarrett T. H. et al., 2011, ApJ, 735, 112

Jeffries R. D., Oliveira J. M., 2005, MNRAS, 358, 13

Kalas P., 2004, in Bulletin of the American Astronomical Society, Vol. 36, American Astronomical Society Meeting Abstracts 204, p. 690

Kastner J. H., Thompson E. A., Montez R., Murphy S. J., Bessell M. S., Sacco G. G., 2012, ApJ, Letters to the Editor, 747, L23

Kennedy G. M., Wyatt M. C., 2012, MNRAS, 426, 91

Kenyon S. J., Bromley B. C., 2005, AJ, 130, 269

Kenyon S. J., Bromley B. C., 2008, ApJ, Supplement Series, 179, 451

Kiss L. L. et al., 2011, MNRAS, 411, 117

Kraus A. L., Shkolnik E. L., Allers K. N., Liu M. C., 2014, AJ, 147, 146

Lagrange A.-M., Backman D. E., Artymowicz P., 2000, Protostars and Planets IV, 639

Lawson W., Feigelson E. D., 2001, in Astronomical Society of the Pacific Conference Series, Vol. 243, From Darkness to Light: Origin and Evolution of Young Stellar Clusters, Montmerle T., André P., eds., p. 591

Lestrade J.-F., Wyatt M. C., Bertoldi F., Menten K. M., Labaigt G., 2009, A&A, 506, 1455

Low F. J., Smith P. S., Werner M., Chen C., Krause V., Jura M., Hines D. C., 2005, ApJ, 631, 1170

Luhman K. L., 2004, ApJ, 616, 1033

Luhman K. L., 2007, ApJ, Supplement Series, 173, 104

MacGregor M., 2014, in IAU Symposium, Vol. 299, IAU Symposium, Booth M., Matthews B. C., Graham J. R., eds., pp. 313–317

Malo L., Artigau É., Doyon R., Lafrenière D., Albert L., Gagné J., 2014a, ApJ, 788, 81

Malo L., Artigau É., Doyon R., Lafrenière D., Albert L., Gagné J., 2014b, ApJ, 788, 81

Malo L., Doyon R., Lafrenière D., Artigau É., Gagné J., Baron F., Riedel A., 2013, ApJ, 762, 88

Mamajek E. E., 2005, ApJ, 634, 1385

Manoj P. et al., 2011, ApJ, Supplement Series, 193, 11

Matthews B. C., Krivov A. V., Wyatt M. C., Bryden G., Eiroa C., 2014, Protostars and Planets VI, 521

Moór A., Kóspál Á., Ábrahám P., Balog Z., Csengeri T., Henning T., Juhász A., Kiss C., 2016, ApJ, 826, 123

Murphy S. J., Lawson W. A., Bessell M. S., 2013, MNRAS, 435, 1325

Nakajima T., Morino J.-I., 2012, AJ, 143, 2

Patel R. I., Metchev S. A., Heinze A., 2014, ApJ, Supplement Series, 212, 10

Pecaut M. J., Mamajek E. E., 2013, ApJ, Supplement Series, 208, 9

Plavchan P., Jura M., Lipscy S. J., 2005, ApJ, 631, 1161

Rhee J. H., Song I., Zuckerman B., 2007, ApJ, 671, 616

Riaz B., Gizis J. E., 2012, A&A, 548, A54
Riaz B., Lodieu N., Goodwin S., Stamatellos D., Thompson M., 2012, MNRAS, 420, 2497
Riviere-Marichalar P. et al., 2014, A&A, 565, A68
Schlieder J. E., Lépine S., Simon M., 2010, AJ, 140, 119
Schlieder J. E., Lépine S., Simon M., 2012, AJ, 144, 109
Schneider A., Melis C., Song I., 2012, ApJ, 754, 39
Shkolnik E., Liu M. C., Reid I. N., 2009, ApJ, 699, 649
Shkolnik E. L., Anglada-Escudé G., Liu M. C., Bowler B. P., Weinberger A. J., Boss A. P., Reid I. N., Tamura M., 2012, ApJ, 758, 56
Sicilia-Aguilar A. et al., 2009, ApJ, 701, 1188
Siegler N., Muzerolle J., Young E. T., Rieke G. H., Mamajek E. E., Trilling D. E., Gorlova N., Su K. Y. L., 2007, ApJ, 654, 580
Simon M., Schlieder J. E., Constantin A.-M., Silverstein M., 2012, ApJ, 751, 114
Smith R., Jeffries R. D., 2012, MNRAS, 420, 2884
Tanabé T. et al., 2008, Publications of the ASJ, 60, 375
Teixeira R., Ducourant C., Chauvin G., Krone-Martins A., Bonnefoy M., Song I., 2009, A&A, 503, 281
Thébault P., Wu Y., 2008, A&A, 481, 713
Theissen C. A., West A. A., 2014, ApJ, 794, 146
Trilling D. E. et al., 2008, ApJ, 674, 1086
Wahhaj Z. et al., 2010, ApJ, 724, 835
Williams J. P., Cieza L. A., 2011, Ann, Rev A&A, 49, 67
Wood K., Lada C. J., Bjorkman J. E., Kenyon S. J., Whitney B., Wolff M. J., 2002, ApJ, 567, 1183
Wright E. L. et al., 2010, AJ, 140, 1868
Wyatt M. C., 2008, Ann, Rev A&A, 46, 339
Zuckerman B., Song I., 2004, Ann, Rev A&A, 42, 685
Zuckerman B., Song I., Bessell M. S., 2004, ApJ, Letters to the Editor, 613, L65
Zuckerman B., Song I., Bessell M. S., Webb R. A., 2001, ApJ, Letters to the Editor, 562, L87

APPENDIX A: OBJECTS WITH $W1-W4>1.0$ AND SNR >5.0, BUT REJECTED FROM THE SAMPLE

In addition to the 19 objects identified with a significant IR excess, there are five objects that have $W1-W4>1.0$ and SNR >5.0, however, they fail criteria (see §2.2) to be included in the final sample. We have included these objects for completeness and interest but note that the SED fits may not be reliable because these objects failed some of the criteria in §2.2 and may have unreliable WISE photometry. These are listed in Table A1 with SED fitting parameters and the reasons for their rejection.

Two of these objects, A_x and B_x, which are probable members of Tuc-Hor (**?**Malo et al. 2013) and BPMG (Malo et al. 2013), respectively, are debris disc candidates (based on $W1-W4$ colour) but had no IR data beyond 25 μm to constrain an SED fit and neither have been identified as having discs in previous work. Two objects, C_x and D_x are both probable members of TWA (Malo et al. 2014b) and have $f_{\rm d}/f_*$ consistent with transitional discs. For object D_x **?** measure $f_{\rm d}/f_*=0.098$, within 1 σ of our measurement and identify a disc 'gap' characteristic of a transitional disc. Object E_x is an ϵ Cha member (**?**) which has a mid-IR SED measured in Fang et al. (2013), who were also unable to measure an absolute $f_{\rm d}/f_*$. Based on the $W1-W4$ colour we suggest E_x is a protoplanetary disc candidate.

APPENDIX B: INDIVIDUAL OBJECTS WITH SIGNIFICANT MID-IR EXCESS

Target A, ES Cha - The $f_{\rm d}/f_*$ value of 0.043 is $\sim 3\sigma$ from the debris disc threshold of 0.01 and is consistent to within 1σ of the $f_{\rm d}/f_*$ value of 0.04 in Gautier et al. (2008).
Target B, EK Cha - This target is reported as a primordial disc in η Cha in Riviere-Marichalar et al. (2014) which is in agreement with our prescription. We measure $f_{\rm d}/f_*=0.118$, within 2σ of the $f_{\rm d}/f_*$ in Gautier et al. (2008), who calculate a value of 0.06. Cotten & Song (2016) measure $T_{\rm d}=140\,$K and $f_{\rm d}/f_*=0.0876$, which would not change the outcome of the disc type based on the analysis in this work.
Target C, ET Cha - The flux fraction calculated in this work is 1.170, $\sim$ triple the value calculated in Gautier et al. (2008). Lawson & Feigelson (2001) categorise this object as a CTTS in η Cha with a primordial disc, in agreement with our judgement.
Target D, RECX 16 - Our SED model yields a flux fraction of 0.175, which is larger than the value of 0.04 calculated in Gautier et al. (2008). Currie & Sicilia-Aguilar (2011) designate this object as a primordial disc, however Rhee, Song & Zuckerman (2007) identify warm dusty material in the disc and suggest it could be either a debris or primordial disc.
Target E, EN Cha - The flux fraction of $0.047^{+0.028}_{-0.016}$ calculated in this work is within 1σ of the value of 0.04 calculated in Gautier et al. (2008). Sicilia-Aguilar et al. (2009) and Currie & Sicilia-Aguilar (2011) identify that the star is a CTTS with a transitional disc, consistent with our classification.
Target F, ϵ Cha 13 - Luhman (2007) identify this object as a WTTS and Manoj et al. (2011) suggest the object has a transitional disc with an inner hole, consistent with our findings.
Target G, TWA 30 - Schneider, Melis & Song (2012) classify it as a debris disc based on photometric IR excess, however, our $f_{\rm d}/f_*$ value of $0.020^{+0.016}_{-0.006}$ is inconsistent with this and we class this objects as transitional. Cotten & Song (2016) have measured $f_{\rm d}/f_*=0.0215$ and $T_{\rm d}=240\,$K, which are both consistent with our measurements to within 1σ.
Target H, ϵ Cha 17 - Based on *Spitzer IRS* spectra, Manoj et al. (2011) measure a class II transitional disc, whereas we suggest a primordial disc.
Target I, ϵ Cha 1 - Our $f_{\rm d}/f_*$ value of 0.455 is larger than the value of 0.280 calculated in Wahhaj et al. (2010). Murphy, Lawson & Bessell (2013) suggest that although Malo et al. (2013) characterise it as a BPMG member, its kinematics are better matched with ϵ Cha (ϵ Cha was not considered in the Malo et al. analysis). Simon et al. (2012) identify this target as a debris disc, however, given the large flux fraction we classify this as a primordial disc source.
Target J, T Cha B - Both the works of Huélamo et al. (2011) and Kastner et al. (2012) identify a transitional disc around this source, in agreement with this work.
Target K, ϵ Cha 10 - The best-fit SED models in

Name (WISE-)	$W1$ (mag)	$W2$ (mag)	$W3$ (mag)	$W4$ (mag, SNR)	$f_{\rm d}/f_*$	Disc Type	Reason
J010335.75−551556.6, A_X	9.03 ± 0.02	8.79 ± 0.02	8.56 ± 0.02	7.86 ± 0.15, 7.4	$> 2 \times 10^{-4}$	D?	1
J044356.87+372302.7, B_X	8.65 ± 0.02	8.56 ± 0.02	8.35 ± 0.02	7.55 ± 0.16, 6.9	$> 1 \times 10^{-4}$	D?	1, 2
J101209.04−312445.3, $C_X^{\rm a}$	7.81 ± 0.02	7.54 ± 0.02	6.14 ± 0.01	4.80 ± 0.03, 39.2	$0.021^{+0.007}_{-0.003}$	T	2
J111027.80−373152.0, $D_X^{\rm b}$	6.60 ± 0.04	6.34 ± 0.02	3.88 ± 0.02	1.73 ± 0.01, 77.5	$0.092^{+0.004}_{-0.010}$	T	2
J120144.32−781926.7, E_X	10.16 ± 0.02	9.74 ± 0.02	8.35 ± 0.02	6.70 ± 0.05, 21.4	$> 4 \times 10^{-3}$	P	1

Table A1. [a]*AKARI* flux (all fluxes quoted as $\times 10^{-14}$ erg/s/cm^2/Å) at $9\,\mu$m = 0.46. [b]*AKARI* flux at 9, 18 and 90 μm = 2.60, 1.28 and 0.02 and *IRAS* flux at 12, 25 and 60 μm =2.06, 0.84 and 0.08. Reasons for rejection: 1. Object has a projected companion with $\Delta K_{\rm s} \leqslant 5$ mag within 16" in 2MASS. 2. The mean photometry of all frames in the L1b catalog for $W1$ and/or $W2$ is $> 2\sigma$ from the value quoted in *AllWISE* (see §2.2).

Fang et al. (2013) are for a thick primordial disc, which we also find.

Target L, 2MASSJ12073346-3932539 - Literature searches for any additional evidence for a disc revealed that this target was the brown dwarf 2M1207, which is host to the giant exoplanet candidate 2M1207b (Mamajek 2005; Barman et al. 2011). Riaz & Gizis (2012) suggest that 2M1207 has a transition disc with an inner disc evacuation due to grain growth/dust settling, however our measurement of $f_{\rm d}/f_* > 1.0$ clearly indicates a primordial disc.

Target M, 2MASSJ08173943−8243298 - This target is reported as a likely new member of the BPMG in Malo et al. (2014b). No previous evidence of disc presence has been found in the literature.

Target N, EI Cha - The flux fraction measured by Gautier et al. (2008) and Cieza et al. (2013) of 3×10^{-4} and 1.6×10^{-4}, respectively, using far-IR data to constrain the SED fit, are slightly below our measured lower limit. We use equation 3 in Backman & Paresce (1993) to calculate $T_{\rm d} \approx 30$ K, which is consistent with our disc temperature upper limit.

Target O, TWA22 AB - TWA22 was initially regarded as a member of the TWA, however subsequent kinematic analyses (e.g., Teixeira et al. 2009; Malo et al. 2013) support a higher probability of membership to the BPMG. No previous work has reported a disc around TWA22.

Target P, TWA 7 - The flux fractions of 2×10^{-3} and 2.5×10^{-3} measured by Low et al. (2005) and Cotten & Song (2016) are in agreement with our measurement to 1 and 2σ, respectively. Low et al. (2005) measure a disc temperature of 80 K, whereas Cotten & Song (2016) model a two-temperature disc with 65 and 220 K components. Both of these are consistent with our $T_{\rm d}$ measurement and the possibility of a debris disc.

Target Q, HD 155555C - **?** find no evidence for IR excess based on $8 - 13\,\mu$m spectroscopy, however, this is not necessarily inconsistent with our detection of a small excess at $22\,\mu$m.

Target R, 2MASSJ17292067−5014529 - Several works support membership to the BPMG (e.g., Kiss et al. 2011; Malo et al. 2014b; Elliott et al. 2016), however, no previous work highlights this object as a disc candidate.

Target S, AU Mic - This target is well-known to have a visually-resolved debris disc (e.g., Kalas 2004; Augereau & Beust 2006; MacGregor 2014). The most recent measurements $f_{\rm d}/f_* = 7 \times 10^{-4}$ and $T_{\rm d} = 65$ K by Cotten & Song (2016) are both within 1σ of our findings.

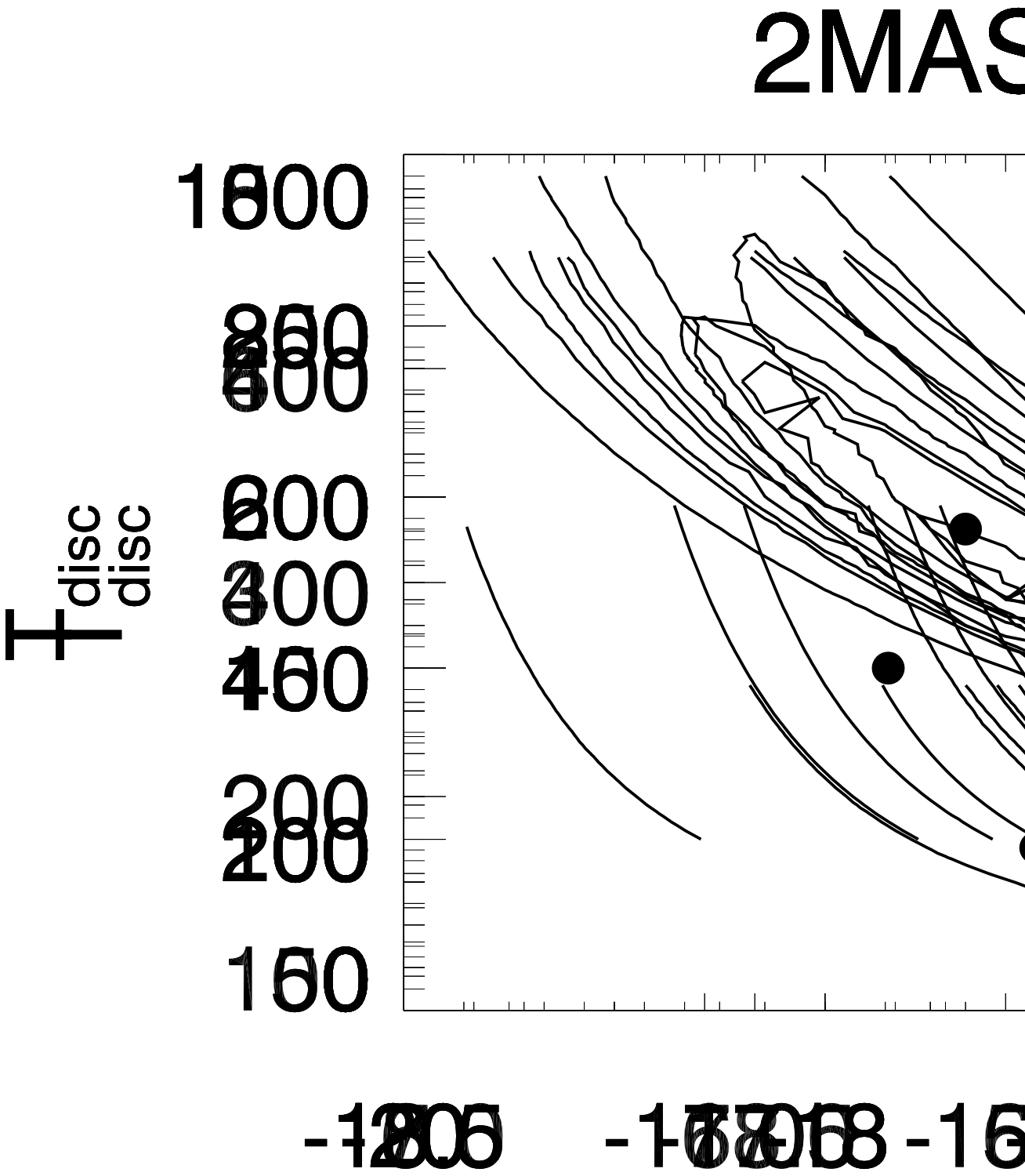
2MAS
disc
disc
1600
1400
1200
1000
800
600
400
200
-1200
-1000
-800
-600
-400
-200